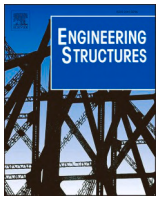
Engineering Structures 317 (2024) 118628



Contents lists available at ScienceDirect

Engineering Structures

journal homepage: www.elsevier.com/locate/engstruct





Flexural strengthening of RC beams using PGFRP bars embedded in strain-hardening cementitious composites (SHCC)

Mohamed Ellithy *, Ali Hassan, Tarek F. El-Shafiey

Structural Engineering Dept., Faculty of Engineering, Tanta University, Tanta, Egypt

ARTICLE INFO

Keywords:
GFRP
Beams
Flexure
Strain hardening cementitious composite (SHCC)
Concrete
Composite

ABSTRACT

The application of the near surface mounted (NSM) fiber reinforced polymer (FRP) as an additional reinforcement at tension side of flexural members is efficient to upgrade the flexural strength. However, this technique must be applied to concrete beams having hard concrete cover to avoid premature failure induced by concrete cover deterioration. The current research aims to improve and evaluate the flexural behavior of reinforced concrete (RC) beams strengthened with embedded prestressed glass fiber reinforced polymer (PGFRP) bars, based on replacement of weak concrete cover with a layer of strain hardening cementitious composites (SHCC). For this investigation, one reference beam (without strengthening) and nine flexural strengthened beams were tested under a four-point bending scheme. All beams had the same reinforcement and geometry, 150 mm width, 300 mm total depth, a total length of 3000 mm and the effective span was 2700 mm. The test parameters were: (1) the strengthening technique (conventional NSM-PGFRP bars, NSM-PGFRP bars covered with external SHCC layer and PGFRP bars embedded in SHCC replaced cover), (2) the prestressing levels in the GFRP bars (0, 10 % and 20 % of the ultimate bar strength) and (3) the thickness of the SHCC layer (30, 40 and 50 mm). Compared to the conventional NSM strengthened beams, the conjunction of SHCC with PGFRP bars not only prevented the spalling of the concrete cover but also increased the load carrying capacity up to 26.5 % and the ductility up to 16 %. A model for the prediction of flexural capacity of the strengthened beams having SHCC replaced cover was conducted, the predicted ultimate loads have a good consistency with the test results.

1. Introduction

Engineers are constantly challenged to develop new repair and rehabilitation techniques for existing structures. Reinforced concrete (RC) structures are particularly susceptible to deterioration due to factors such as chloride penetration, high humidity, and marine environments. The construction industry needs to find non-corrosive alternatives to steel reinforcement, or ways to better protect steel and concrete from corrosion. Generally, fiber reinforced polymer (FRP) has become one of the most efficient strengthening materials in comparison with the conventional steel reinforcement. The FRP composites are distinguished with an outstanding material characteristics such; corrosion-resistance, low cost of maintenance, high strength to weight ratio and easy handling in construction [1–14]. Regarding recent research works as well as field applications, the main four efficient alternatives to steel reinforcement are Aramid, Basalt, Carbon, and Glass Fiber Reinforced Polymers (AFRP, BFRP, CFRP and GFRP). Recently, the high tensile structural adhesives have become more available, therefore, repair of RC structures using the externally bonded (EB) FRP plates/-sheets is an effective technique for repair/strengthening of several defected structural elements [15–22]. The repair/strengthening method can be also applied by embedment of FRP strips/bars in RC elements, namely, the near-surface mounted (NSM) technique [22–28].

Although FRP composites have several benefits in strengthening/repair of RC structures, the FRP composites still have drawbacks in application. For most FRP flexural strengthened structures, the governing factor that leads to premature failure is debonding induced by deterioration/spalling of concrete cover. Using anchorages for EB strengthened/repaired flexural members could increase strength by about 20 % as it transforms the epoxy bonding failure to anchorage failure [29–31]. Anchorage of externally bonded CFRP sheets/plates were typically used to postpone the bond induced failure. These anchors generally have higher delamination load than their counterparts without anchors [32]. Increasing the number of anchors significantly enhanced the flexural response of the strengthened beams in terms of the utilized strain of the FRP laminates, the utilization percentages

* Correspondence to: Structural Engineering Dept., Faculty of Engineering, Tanta University, Tanta 31511, Egypt.
E-mail address: Mohamed.ezat@f-eng.tanta.edu.eg (M. Ellithy).

https://doi.org/10.1016/j.engstruct.2024.118628
Received 25 November 2023; Received in revised form 29 June 2024; Accepted 13 July 2024
Available online 23 July 2024
0141-0296/© 2024 Elsevier Ltd. All rights are reserved, including those for text and data mining, AI training, and similar technologies.

regarding the test results were 27 %, 61 %, and 99 %, for the control unanchored, having two anchors, and having four anchors, respectively [33]. In comparison with the other strengthening techniques, the NSM has been proven to better utilize bonded FRP materials [34–37]. Since EB technique mainly requires using anchorages which means additional costs and efforts, the NSM technique has attracted the attention as an efficient alternative instead of EB method. The NSM method has proven several gains over the EB method such higher bond efficiency in addition to improved protection of the FRP reinforcement [38]. Although the NSM FRP bars/strips have a relatively strong bond with concrete, failures governed by debonding are still likely to take place in RC beams strengthened/repaired in flexure. Debonding induced failure could be either an interfacial debonding between the adhesive material and the substrate concrete or in the form of separation/spalling of concrete cover in which the NSM FRP bars/strips are embedded [38]. As per previous research, the cracking pattern regarding to debonding mode of failure could be in two forms, the intermediate crack induced debonding [39,40] at which the debonding of the FRP is triggered from the maximum moment zone then extends to the ends. The end debonding failure [41–43] at which the debonding of the FRP begins from one end of the beam then propagates to the maximum moment zone. To count four the most common failure modes of NSM flexural strengthened beams, Jung et al. [44] studied the failure modes of 106 RC strengthened beams in flexure from previous research using NSM FRP reinforcement. It was found that strengthened beams failure took place due to: 1) For 55 % of specimens, delamination of concrete cover in which the original tensile steel bars played as a bond breaker, and separation of the concrete cover was attained; 2) For 35 % of specimens, FRP rupture at the maximum-moment zone; 3) For 10 % of specimens, bond failure was recorded at the filler-to-concrete interface. Regarding literature, the most common mode of failure of NSM FRP flexural strengthened beams is induced by debonding.

Previous research works studied the main parameters that effect on the bond strength of FRP bars/strips mounted to the substrate concrete by NSM technique. It was found that the bond of NSM FRP strips was enhanced by increasing the FRP aspect ratio (strip width/strip thickness) [45]. Bilotta et al. [46] reported that using low strength concrete made most NSM FRP specimens show an interfacial concrete-adhesive failure at low ultimate pull-out load. The ultimate pull-out load of NSM FRP system rises by increasing the FRP bonded length, however, this increase is insignificant by increasing the bonded length over the critical bond length [47–49]. The type of the used adhesive material is also a key parameter that affects the NSM FRP bond behavior, Shehab et al. [50] and Al-Mahmoud et al. [51] concluded that using epoxy adhesive gives better experimental results comparing to the cement adhesive. The grove size used for NSM also has a tangible impact on the bond efficiency between FRP and the substrate concrete. Novidis and Pantazopoulo [40] and De Lorenzis [48] reported that for a certain bonded length, the failure load increases with increasing groove depth. To avoid premature bond failure of FRP strips/bars used for NSM strengthened/repaired elements, ACI Committee 440.2R-08 [52] recommended minimum width and depth of the NSM grooves.

Several researchers tried to overcome the deterioration in concrete cover which causes bond induced failures. Several research efforts have been carried out to utilize the prestressing for FRP flexural strengthened beams as a prestressed FRP system can integrate/exploit the advantages of both methods of strengthening to upgrade the ultimate flexural capacity and can enhance the cracking behavior [53–55]. Sabau et al. [56] experimentally studied a comparison between bottom and side mounted NSM bars, almost similar ultimate load capacities were attained also the concrete cover detachment was avoided. Haddad and Yaghmour [57] also studied side NSM CFRP strips having trapezoidal and parabolic profiles, this configuration limit/prevent the spread of separation of concrete cover. The flexural strengthened beams using NSM CFRP strips having FRP U-jackets located at or near the end of the NSM strips effectively delayed debonding failure [58]. Khalil et al. [59] employed precast reinforced plates made of Strain Hardening Cementitious Composites (SHCC) to strengthen a one-way slab with cut-outs at tension side, these plates were mounted to the slab with epoxy adhesive and surface preparation by NSM technique. By using this technique, the debonding of the SHCC plates was avoided until the failure. Afefy et al. [60] used another technique, the weak cover was completely removed and the whole cover was replaced with Engineered Cementitious Composites (ECC) prior to the application of CFRP sheet at tension side. This technique employed the ECC with high tensile and bond strengths to transmit the tensile force of the CFRP sheets to the strengthened beam, the ECC layer controlled the concrete cracking and avoided premature bond induced failure. SHCC can be considered as a new generation of high-performance fiber reinforced cementitious mortars. The SHCC was employed by many researchers regarding its outstanding mechanical properties. The superior material characteristics of the SHCC can be achieved by intentionally engineered three phases: matrix, fiber, and matrix/fiber interface, pertaining to the theory of micromechanics [61–64]. Pertaining to the tensile strength, the SHCC exhibits a high strain capacity (more than 3 %), this strain capacity is about a hundred times of the maximum tensile strain value of the ordinary concrete [65]. Furthermore, a single localized fracture crack took place in conventional concrete under tension is switched to multiple micro-cracks (crack width below 100 μm) for its counterpart of SHCC [66,67]. These multiple micro-cracks in SHCC can enhance the damage pattern of the SHCC-concrete composite members [68–70]. The SHCC showed a good bond and composite action with concrete, RC members in flexure and shear were strengthened with external SHCC layer without any SHCC-concrete separation until failure of specimens [70–73].

Regarding previous work, the bond induced failure accompanied with the FRP NSM strengthened RC members is a problem that results in a premature failure with lower ultimate capacity than expected. The bond failure is also a barrier to guarantee the maximum exploitation of the FRP additional reinforcement for the strengthened members. In this study, GFRP reinforcement is added to the tension side of RC beams in form of NSM to upgrade its flexural strength. A solution for debonding induced problems was studied by replacing the weak concrete cover with a layer of SHCC in which the additional GFRP reinforcement was embedded. In the current research, the SHCC is recommended due to its outstanding characteristics such compatibility and composite action with concrete, high tensile strength, high strain capacity that could be compatible with the GFRP, enhancement of cracking behavior and its ability to form a protection layer for beam's reinforcement against harsh environments. The studied parameters were the technique of strengthening, prestressing level of the GFRP bars, and the thickness of the SHCC layer. The effect of these parameters on modes of failure, ultimate capacity, ductility, and cracking were also discussed. For design purposes, a prediction model to calculate the ultimate capacity of the strengthened beams having SHCC replaced cover was conducted and the predicted ultimate loads were compared to the experimental results.

2. Experimental program

2.1. Test specimens and the studied parameters

The experimental program involved ten beam specimens having strong-shear/weak-bending capacities and were designed according to ACI318–19 [74]. As shown in Fig. 1-a, all beams had the same reinforcement and geometry, 150 mm width, 300 mm total depth, a total length of 3000 mm and the effective span was 2700 mm. The longitudinal main reinforcement included two steel rebars of 16 mm diameter (D16) which were placed at the tension side of the RC beam, while two steel rebars of D12 were located at the compression side of the RC beam. The tests were carried out in a four-point bending test, the pure bending length within the two loading points was 600 mm. The targeted mode of failure of the beams was flexural failure, therefore, to avoid shear failure, densely arranged stirrups were designed then added at the shear

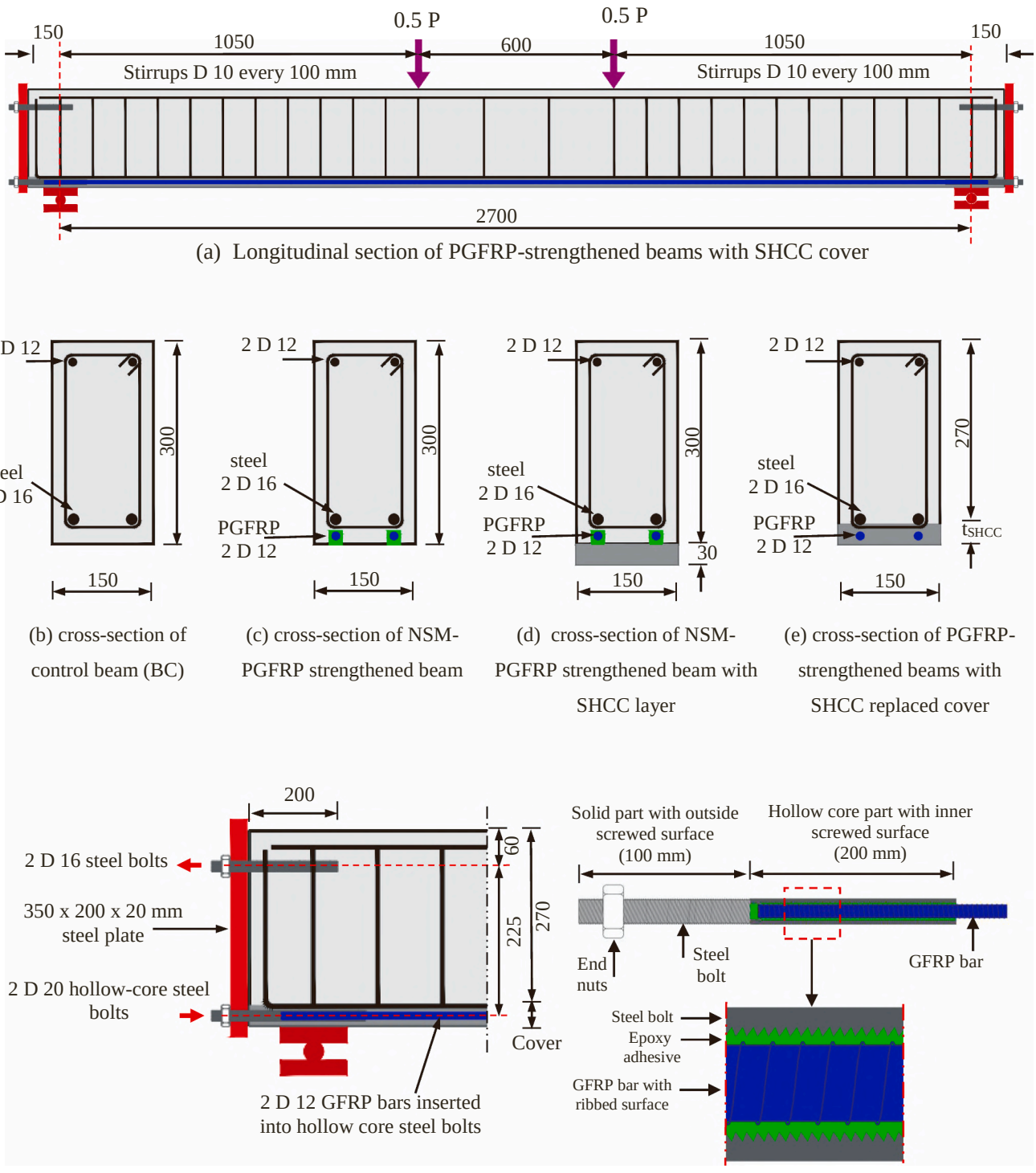


Fig. 1. Details of the tested beams (All dimensions in mm).

zone. The stirrups at the shear zone had a diameter of 10 mm and were arranged with a spacing of 100 mm, while two D8 stirrups were placed at the zone of pure moment, as depicted in Fig. 1-a.

As listed in Table 1, the tested specimens were classified into three groups via test parameters; Group 1: the strengthening techniques, Group 2: the prestressing level and Group 3: the thickness of the SHCC layer. The effect of several strengthening techniques was studied in Group 1; the first technique was adding prestressed/non-prestressed GFRP bars at tension side in form of NSM, as shown in Fig. 1-c. The second technique was applying NSM PGFRP bars covered externally with SHCC layer, as shown in Fig. 1-d. The rational of the second technique is to evaluate the ability of the external SHCC layer to prevent the potential spalling of the original cover. In the third technique, the concrete cover was completely replaced by SHCC layer in which the PGFRP bars were embedded, as shown in Fig. 1-e. For all beam specimens of Groups 2 and 3, the strengthening procedure of the third technique was followed. The effect of the prestressing level was studied in Group 2, the prestressing level (the pre-stress of the GFRP bar is

Table 1
Description of the tested specimens.

Group	Beam	P_s, %	t_{SHCC}, mm	Objectives
Control	BC	–	–	Reference beam
Group 1	B−0 %-N − 0	–	–	Effect of strengthening technique
	B−20 %-N − 0	20	–	
	B−20 %-NS−30	20	30	
	B−20 %-S−30	20	30	
Group 2	B−0 %-S−30	0	30	Effect of prestressing level
	B−10 %-S−30	10	30	
	B−30 %-S−30	30	30	
Group 3	B−20 %-S−40	20	40	Effect of SHCC thickness
	B−20 %-S−50	20	50	

P_s = prestressing level regarding to the ultimate capacity of the GFRP bars; tSHCC = thickness of the SHCC layer; BC= the unstrengthened control beam; B=the strengthened beam; N = using NSM-GFRP bars, NS = using NSM-GFRP bars covered by SHCC layer; S = GFRP bars embedded in the SHCC layer replacing the concrete cover.

divided by its maximum strength) varied from 0 % to 30 %, as listed in Table 1. In Group 3, the effect of the SHCC replacement thickness was evaluated, and the studied thicknesses were 30, 40 and 50 mm. In the current study, the adopted clear concrete cover was 25 mm, therefore the replacement depth of the cover was 30 mm to expose the half diameter of the stirrups as it would be more beneficial for bond behavior that the SHCC should contact a rough hard surface with prominent transverse bars [75]. As shown in Table 1, the designation of the beam specimens reflects the studied parameters, the letters "BC" indicated the unstrengthened control beam. On the other hand, the strengthened beams are designated by four symbols separated by dashes. The first symbol (B) refers to a strengthened beam, while the following percentage refers to the prestressing level. The third symbol stands for the strengthening technique (N = NSM-GFRP bars, NS = NSM-GFRP covered by SHCC layer and S = GFRP bars embedded in the SHCC layer). Eventually, the number following the strengthening technique is the thickness of the SHCC layer in mm.

2.2. Materials

A ready mixed normal strength concrete was used in the construction of the tested beams. The mix components contained; ordinary Portland cement with grade of 42.5 N (type-I), crushed limestone (the maximum aggregate size is 10 mm), sand and water, as listed in Table 2. The mixture ingredients of the strain hardening cementitious composite (SHCC) are summarized in Table 2. The SHCC mixture contained; ordinary Portland cement with grade of 42.5 N (type-I), fine aggregate, silica fume (silica fume to cement ratio of 0.18, by weight), fibers (polypropylene fibers), water (water-to-binder ratio W/B of 0.20, by weight) and water-reducing admixture. To assure the behavior of the strain hardening with multiple micro-cracking, the fracture toughness of the matrix must be minimized [76]. Therefore, for mixing of the SHCC, the fine aggregates only are suggested to be used (silica sand with a normal maximum size of 1.00 mm). High-strength polypropylene (PP) fibers with diameter of 25 μm and length of 12 mm were used in the SHCC mixture with a volume fraction of 2 %.

In the test date of each beam, material tests of the concrete were performed on twelve standard cylinders of size 150 × 300 mm. Six cylinders were tested under uniaxial compression as per ASTM C39/C39M [77], while splitting tensile tests were performed on the other cylinders. All beams were tested in the same week, therefore the compressive/tensile strengths showed almost similar results for all beams. For all tested cylinders, the average compressive strength was 25.6 MPa, while the average splitting tensile strength was 3.2 MPa. Six cylinders having a size of 50 × 100 mm were tested under uniaxial compression to determine the compressive strength of the used SHCC according to JSCE recommendations [78]. The average compressive strength of the tested SHCC cylinders was 61.3 MPa. Direct tension tests were executed on six specimens to determine the tensile strength of the used SHCC. It was recommended to carry out the axial tension test on real scale specimens to avoid the size effect [79]. The dimensions of the tested dog-bone specimens under direct tension are shown in Fig. 2. The average value of the first cracking and ultimate strengths based on the results of the tensile tests were 4.7 and 6.9 MPa, respectively. Fig. 3 shows the SHCC tensile stress-strain relationship of a tested specimen.

The tensile properties of the used reinforcing bars (steel/GFRP) are listed in Table 3. B420DWR is the type of the used steel bars with diameter 12 and 16 mm, while B240D-P is the type of steel bars with 8 mm diameter. For each bar's diameter, six samples were tested under axial tension in accordance with ASTM Standard (ASTM A370–19) [80]. The average yield and ultimate tensile strengths for steel bars of type B420DWR were 423 MPa and 645 MPa, respectively. The average yield and ultimate tensile strengths for steel bars of type B240D-P were 243 MPa and 357 MPa, respectively. The tensile tests were also

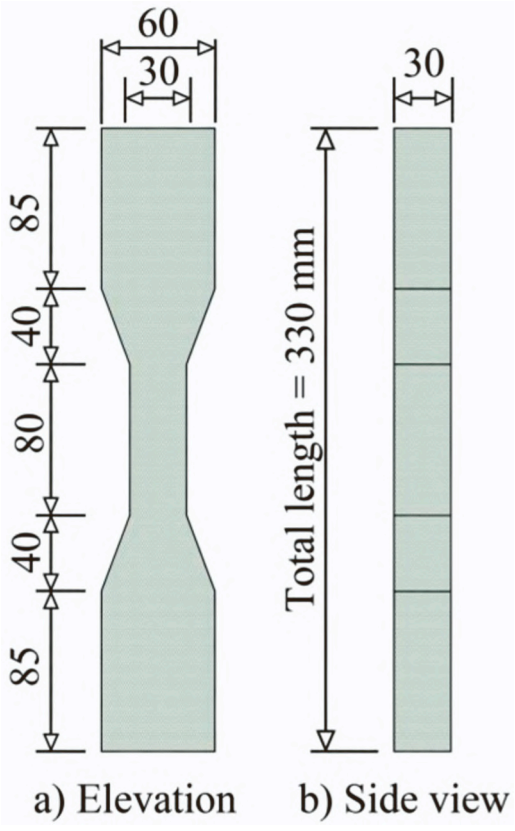


Fig. 2. Dimensions of the specimen of the SHCC uniaxial tensile test, dimensions in mm.

Table 2
Mix ingredients for the used concrete and SHCC per cubic meter (kg/m^3).

Material	Cement	Sand	Coarse aggregate	Silica fume	Fibers (volumetric ratio)	Super plasticizers	Water	Water-to-binder ratio
SHCC	1342	157.9	—	237	16.20 (2.0 %)	31.6	312.1	0.20
Concrete	350	530	1300	—	—	—	175	0.5

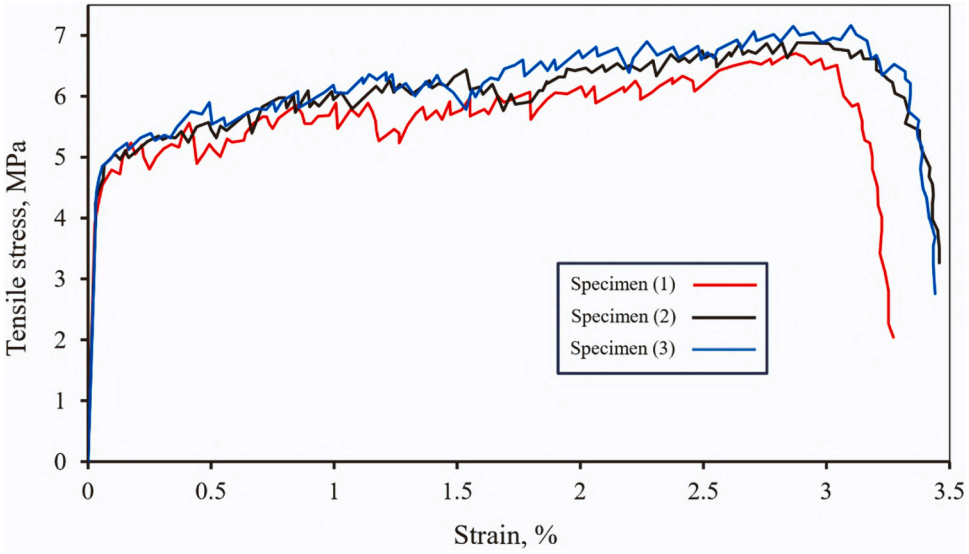


Fig. 3. Stress-strain curve of three specimens of the SHCC under uniaxial tension.

Table 3
Tensile properties of the reinforcing bars.

Nominal bar diameter (mm)	Material type	Average yield/proof stress (MPa)	Average tensile strength (MPa)	Average modulus of elasticity (GPa)
8	Steel B240D-P*	243	357	200
12	Steel B420DWR*	420	639	203
16	Steel B420DWR*	426	651	203
12	GFRP	———	1013	33

performed on six test samples of the used glass fiber reinforced polymer (GFRP) bars with diameter of 12 mm, the tensile strength as well as the modulus of elasticity were conducted in consistence with ASTM Standard (ASTM D7205–06) [81]. Fig. 4 shows the tensile stress-strain curves of the tested samples of the used GFRP bars, the average tensile strength of the tested bars was 1013 MPa, while the average maximum strain was 30,300 microstrain. Epoxy mortar (MasterBrace ADH 2200) was selected as an adhesive material to bond the GFRP bars to the concrete. According to the manufacturer's datasheet, the density of the used epoxy mortar is 1.85 kg/L and its setting time is 12 h. The used epoxy requires at least 7 days to reach its full strength. The compressive, tensile and flexural strengths of the used epoxy are about 65, 10 and 20 MPa, respectively. As per the manufacturer's report, the bond strength can be reached by the used epoxy is more than 2.00 MPa.

2.3. Procedure of strengthening

In the current study, three strengthening schemes were used, namely, conventional NSM-PGFRP bars, NSM-PGFRP bars covered with external SHCC layer and PGFRP bars embedded in SHCC replaced cover. Before the application of the strengthening, some primary preparations were required then the strengthening procedure could be performed. The following sections present in detail the strengthening procedure of each technique. Also, the details of the strengthening procedure are shown in Fig. 5.

2.3.1. Primary preparations

As shown in Fig. 5-b, the ends of the GFRP bars were prepared by attaching to a screwed hollow core steel bolt (D20) using epoxy with embedded length of 200 mm [82], the steel bolts had a solid part with a

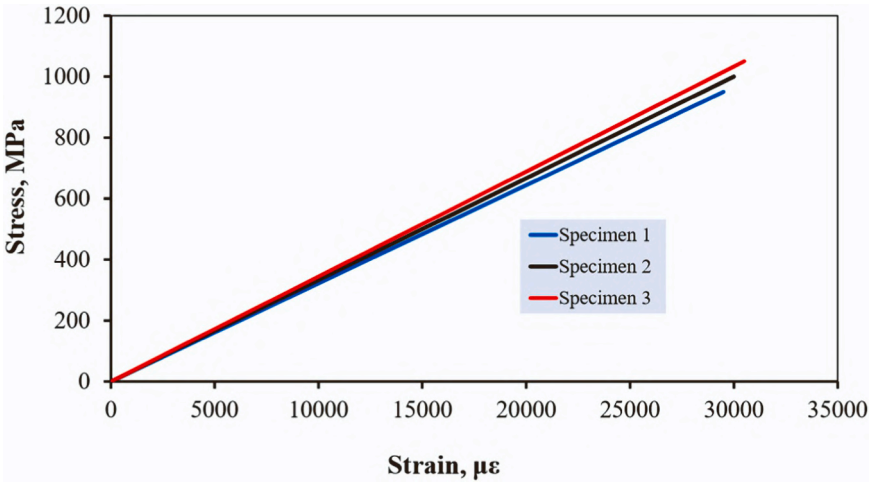


Fig. 4. Stress-strain curves of three GFRP bars under uniaxial tension.



Fig. 5. strengthening processes.

length of 100 mm. The screwed hollow cores of the steel bolts were cleaned to remove any traces of water, oil, and dust, then were filled to their middle depth with epoxy. The GFRP bars were then placed into them for a minimum of seven days (The required period to reach the full strength of the used epoxy). These prepared ends were used lately to apply the prestressing force. The safe embedment length of the GFRP bars attached to hollow core steel bolts was conducted via testing GFRP attached bars using the same described configuration under axial tension until rupture of the GFRP bars. Several trials were carried out until reaching the safe embedment length (200 mm). As shown in Fig. 1-f and 5-a, two steel bolts were planted using epoxy with embedded length of 200 mm at the ends of all beams, these bolts were used to fix the steel

plate to the end of the beam. The pullout force acting on the epoxy planted steel bolts was calculated based on the reaction of the anchor steel plate on these bolts due to the eccentric prestressing force. Then the bolt's embedded length was calculated regarding ACI318–19 chapter 17 [74], considering high safety margin to avoid any slippage during testing.

2.3.2. Conventional NSM-PGFRP bars

1. Along the beam's length, grooves were cut within the concrete cover at the tension side, then the loose particles in the grooves were carefully removed, as shown in Fig. 5-a.
2. Anchoring steel plates (the plate thickness is 20 mm) were attached to the planted steel bolts shown in Fig. 5-a. at the ends of each beam.
3. The beam's grooves were half-filled with epoxy, then the prepared GFRP bars were placed inside them. Simultaneously, the prepared steel ends were inserted through holes at the end of the anchoring plates. Afterwards, the pretension tensile force was applied using the hydraulic jack while monitoring the strain level of the GFRP bar, as shown in Fig. 5-d.
4. Finally, the whole grooves were refilled with epoxy, then the live-end of the GFRP bar was fixed to the steel anchor to maintain the pre-tension prestressing force, as shown in Fig. 5-c.

Note that, before the final fixing to the anchor steel plate, the strain level of the GFRP bars was recorded to compensate any strain decreases induced by the short-term losses to achieve the required prestressing force.

2.3.3. NSM-PGFRP bars covered with external SHCC layer

In this technique, the same steps presented in Section 2.3.1 were followed, in addition after the application of the PGFRP bars, externally bonded SHCC layer of 30 mm thickness was cast then cured by wet cloth for 14 days. The details of the strengthening are shown in Fig. 1-d.

2.3.4. PGFRP bars embedded in SHCC replaced cover

1. The whole concrete cover at tension side was removed carefully. Getting a rough surface was considered during the removal of the concrete cover to guarantee a perfect interfacial bond between the concrete and the SHCC layer.
2. The anchoring steel plates were attached to the epoxy planted steel bolts at beam's ends.
3. The prepared ends of the GFRP bars were inserted throw the holes of the anchoring plates, then the pretension force was applied by the hydraulic jack, as shown in Fig. 5-d.
4. The strain level of the GFRP bars was monitored for 1 hr. to balance any strain decreases induced by the short-term losses, then the live-end of the GFRP bar was fixed to the anchoring steel plate, as shown in Fig. 5-e.
5. Finally, the SHCC layer was cast over the PGFRP bars replacing the removed concrete cover then this layer was cured with wet burlap for 14 days.

2.4. Test setup and instrumentations

Fig. 6 shows the setup of the four-point loading test. A series of 100 mm linear variable displacement transducers (LVDTs) were used to record the vertical deflection at the mid-span point, under the loading points, and over the two supports of the tested beams. Also, 10 mm electrical strain gauges were utilized to measure the developed strain levels in the longitudinal steel reinforcing bar and the GFRP bar. An optical microscope of 0.01 mm accuracy was employed to measure the width of the main crack. For all beams, two concentrated loads were applied at 1050 mm from the supports. A load cell with capacity of 200 kN was used to measure the acting load. A series of 100 mm Pi-gauges were employed to obtain the longitudinal strain distribution along the beam's depth. Four Pi-gauges were uniformly placed along the beam's depth as well as one Pi-gauge was placed at the center of the SHCC layer, as shown in Fig. 6. The LVDTs, electrical strain gauges, Pi-gauges as well as load cell were all connected to an automatic data logger system to collect and arrange the recorded data.

3. Experimental results

3.1. Crack patterns and modes of failure

The cracking pattern at failure for the control and the strengthened beams are shown in Figs. 7–10. For all beams, the first flexural crack was observed within the middle-third (maximum moment zone). By increasing the load, the crack width increased simultaneously with initiation of several flexural cracks along the beam. Afterwards, these flexural cracks propagated towards the flexural compression zone. Finally, the control beam failed by yielding of the main flexural steel followed by concrete crushing at compression zone (tension failure). However, all other beams failed after yielding of the main tensile steel followed by concrete crushing at compression zone but without rupture of GFRP bars (compression failure).

For strengthened beams with non-replaced cover in Group 1, it was noticed that a significant widening of flexural cracks was attained after yielding of the main steel. Also, additional steep cracks started to propagate out of the middle third between the flexural-shear cracks as shown in Fig. 8. These cracks started to propagate from the edge of the

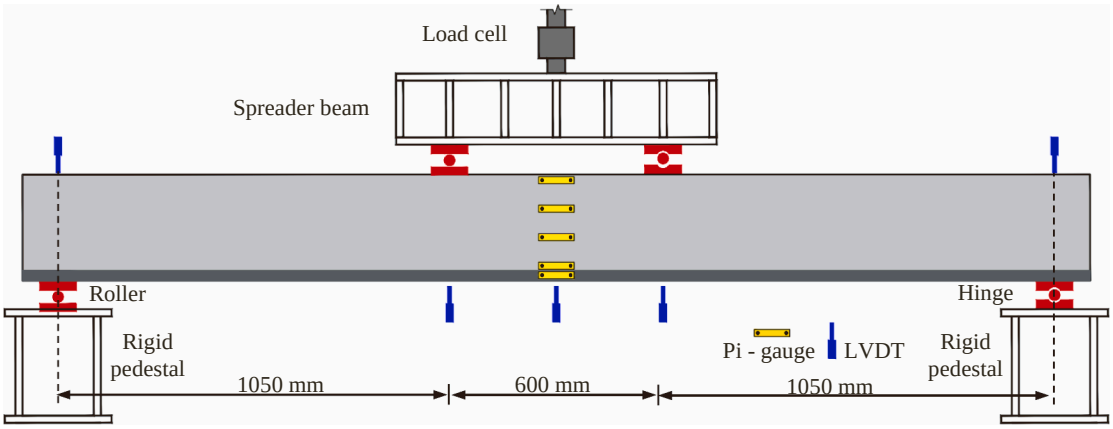


Fig. 6. Test setup and instrumentation.

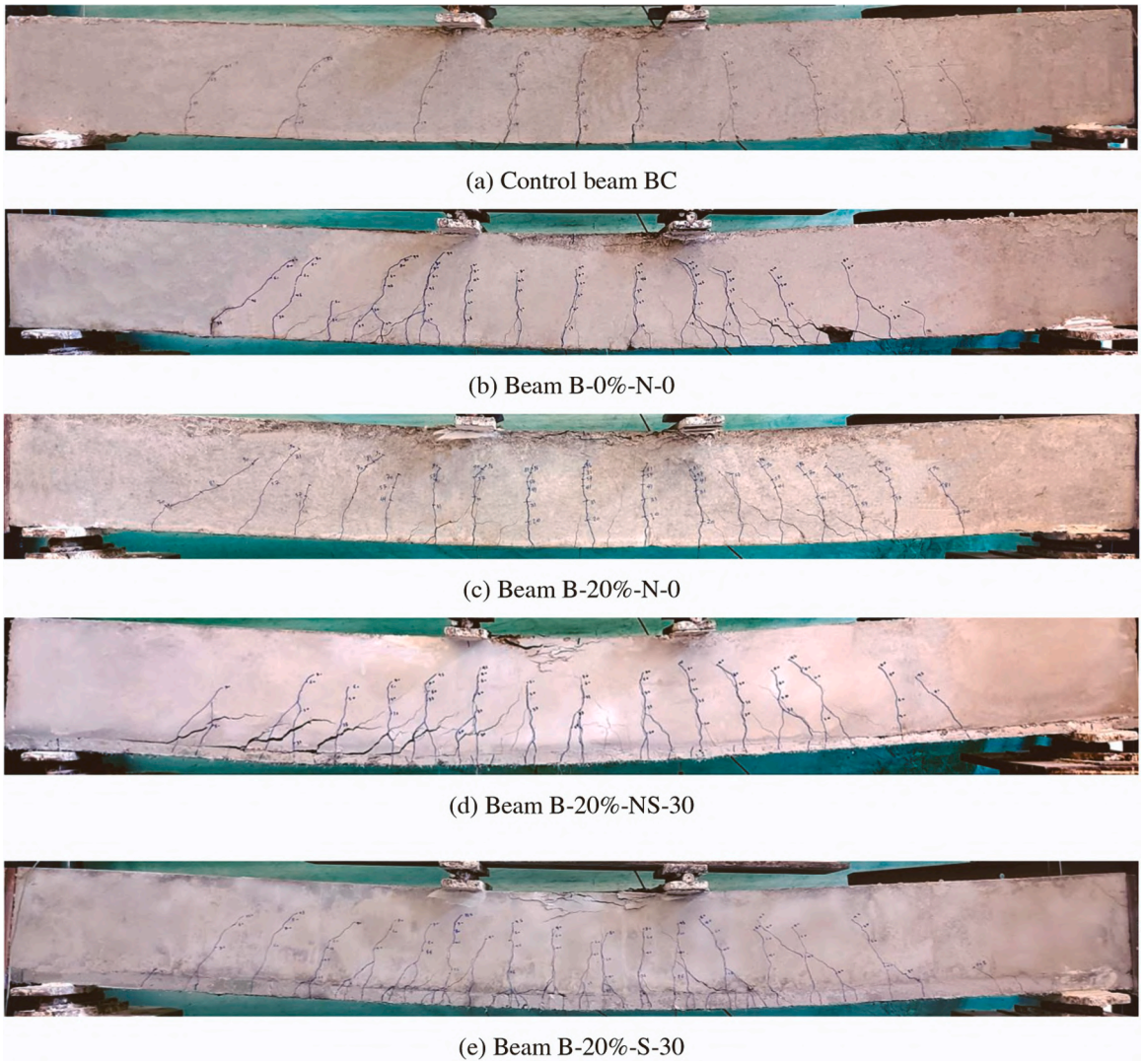


Fig. 7. Cracking patterns at failure of the control beam and the beams of Group 1.

maximum moment zone then extended towards the supports. The steep cracks propagated where the bond stress between the NSM GFRP bars and the substrate concrete is maximum. Post to steel yielding, the low elastic modulus of the GFRP caused an extensive elongation of the GFRP bars which could not be resisted by the weak concrete cover causing initiation of these steep cracks. The released energy due to the elongation caused deterioration and spalling of concrete cover, as shown in Fig. 8. Although severe deterioration took place in the concrete cover zone of the beams strengthened without cover replacement, the failure was not governed by debonding of GFRP reinforcement. This was attributed to the role played by the steel plates used to attach the GFRP bars which represented an end-anchoring and prevented the full-debonding of the GFRP bars. The steel plates (end-anchors) made these beams act as unbonded prestressed beams as the GFRP bars were relatively free to elongate, this behavior also coincides with previous research work [83].

For beams strengthened with SHCC replaced cover in Groups 2 and 3, it was observed that the SHCC replaced cover showed numerous well distributed flexural cracks. As shown in Figs. 7, 9 and 10, for all beams of Groups 2 and 3, regardless of the prestressing level or the SHCC thickness, the deterioration and spalling of concrete cover was not attained until the complete failure. This manner assures the efficiency of the newly developed technique compared to the other techniques followed in Group 1. The SHCC replaced cover played two significant roles. Firstly, the ultimate tensile strain of the SHCC (more than 0.03) is compatible with the maximum strain capacity of the used GFRP, therefore it could resist the extensive elongation attained by the GFRP bars. Secondly, the SHCC layer has a perfect interfacial bond with the substrate concrete which enhanced the composite action, eliminated any relative slippage and acted as a perfect transition layer [70–73]. It is worth mentioning that, due to minor shuttering imperfections during casting of the SHCC layer, nonconformity was observed in some places at the outer surface of the SHCC-concrete interface. This nonconformity was surficial and did not affect the crack pattern of the beams strengthened with SHCC replaced cover as the SHCC cover did not spall and no post-yield steep cracks were observed at the SHCC layer. Based on the visual inspection and the measured longitudinal strains along depth (see Section 3.7), no separation was recorded between the substrate concrete and the SHCC replaced cover.

3.2. Load-deflection behavior

The cracking, yield, and ultimate loads in addition to the corresponding deflections are summarized in Table 4. The maximum deflection in this research is the deflection at the ultimate load for all beams. For the control beam, the load–deflection curve was characterized by three consequent stages. The first stage ended with the first flexural crack at the tension side then the beam's stiffness started to

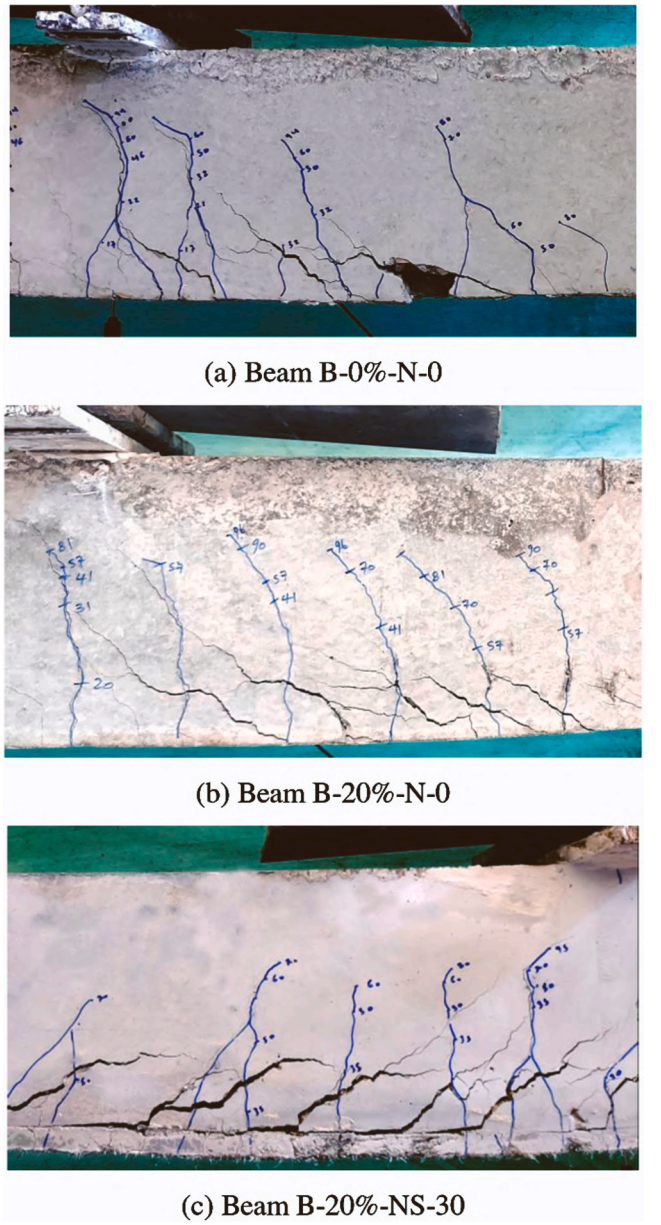


Fig. 8. Spalling of the non-replaced concrete cover of strengthened beams of Group (1).

decay. The second stage continued with lower stiffness until reaching the yield point of the main steel. The control beam failed at the third stage by yielding of the main steel followed by concrete crushing at compression zone, therefore, it showed a long plateau indicating a ductile manner. Although all other beams showed the same behavior of the control beam until yield point, these beams failed suddenly at the third stage while the load was increasing (load hardening) without showing a plastic behavior. This was caused by the different mode of failure as the other beams failed due to concrete crushing at compression zone without rupture of the GFRP bars (compression failure).

The load-deflection curves of Group 1 are shown in Fig. 11. B-0 %-N-0 without replacement of concrete cover without prestressing showed 25.6 % higher ultimate load compared to BC but with maximum deflection lower than BC by 11 %. By applying a prestress with level of 20 %, B-20 %-N-0 recorded 38 % higher ultimate load, 39 % lower deflection comparing to the control beam, also a significant increase in the beam's stiffness was noticed compared to B-0 %-N-0. For beam B-20 %-NS-30, the 30 mm additional external SHCC layer increased the beam's depth and stiffness compared to the other beams. This increase in stiffness entailed 50 % higher load carrying capacity than that of the reference beam, however, the maximum deflection recorded approximately the same deflection recorded by B-20 %-N-0. By comparing B-20 %-N-0 and B-20 %-NS-30, the stiffness and the ultimate capacity of the later showed a slight increase which can be explained that the additional SHCC layer without cover replacement did not avoid the spalling and deterioration of the concrete cover and the same premature debonding induced failure was noticed. The visual inspection and the measured longitudinal strains along beam's depth (see Section 3.7) assured that a separation between the SHCC layer of B-20 %-NS-30 and the substrate concrete was attained which finally did not protect the beam from deterioration of the concrete cover. B-20 %-S-30 exhibited 74 % higher ultimate load compared to BC with maximum deflection lower than BC by 30 %.

Compared to B-20 %-N-0 and B-20 %-NS-30, the SHCC replaced cover of B-20 %-S-30 not only eliminated the spalling of concrete cover but also enhanced both the ultimate load and the maximum deflection. It is obvious that all 20 % prestressing level strengthened beams of Group 1 had a convergent stiffness until yield load, then the slope of the load-deflection curve of beams with non-replaced cover became steeper than that of B-20 %-S-30 until failure. This was due to the severe deterioration took place in the non-replaced cover post to steel yielding which caused a partial debonding (see Section 3.1) and made these beams without cover replacement to act as unbonded prestressed beams with lower stiffness and ultimate capacity [83]. Previous research work reported that the ultimate flexural capacity of prestressed unbonded beams decreased by about 20 % than that of bonded beams [84,85]. In the current research B-20 %-N-0 and B-20 %-NS-30 acted as unbonded prestressed beams, the recorded load carrying capacity reduced by 20.5 % and 14 %, respectively, compared to B-20 %-S-30 with replaced concrete cover.

The load-deflection curves of Group 2 are shown in Fig. 12. By comparing to the reference beam (BC), the ultimate load of B-0 %-S-30, B-10 %-S-30, B-20 %-S-30 and B-30 %-S-30 increased by 59 %, 69 %, 74 % and 88 %, respectively, while the maximum deflection reduced by 4 %, 18 %, 30 % and 34 %, respectively. It is obvious that by increasing the prestressing level, the ultimate load-carrying capacity as well as stiffness increase while the ultimate deflection decreases. The load-deflection relationships of Group 3 are presented in Fig. 13. By comparing to the control beam, the ultimate load of the beams B-20 %-S-30, B-20 %-S-40 and B-20 %-S-50 increased by 74 %, 82 % and 90 %, respectively, while the maximum deflection reduced by 30 %, 34 % and 31 %, respectively. It was observed that B-20 %-S-50 recorded only 8 % higher ultimate load than that of B-20 %-S-30 showing approximately the same ultimate deflection. The ultimate load capacity and stiffness increase by increasing the thickness of the SHCC replaced cover, however, this increment is not significant and the thickness of 30 mm of the SHCC replaced cover can be considered as a sufficient thickness.

3.3. Deflection-based ductility

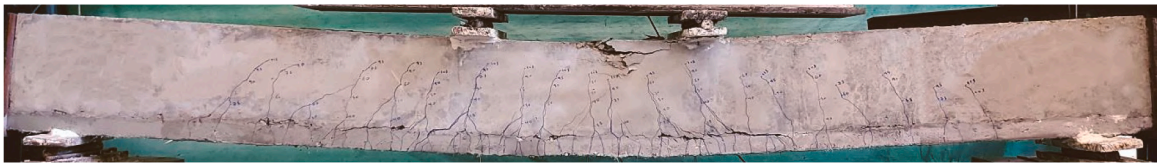
Many approaches have been used to express the ductility of RC members subjected to flexure. In this study, since the yield of the main steel had a significant effect on the load-deflection relationships, a deflection-based approach is adopted. The deflection-based ductility index [86] can be expressed as follows:

$$\mu_d = \frac{\Delta_u}{\Delta_y} \quad (1)$$

Where; μ_d= Deflection-based ductility index, Δ_u= the maximum deflection at ultimate load, Δ_y= the deflection pertaining to the yield of main steel. The deflection-based ductility indices of all tested beams are presented in Table 4. Generally, using any strengthening at tension side that made the flexural member to fail by crushing of concrete at



(a) Beam B-0%-S-30



(b) Beam B-10%-S-30

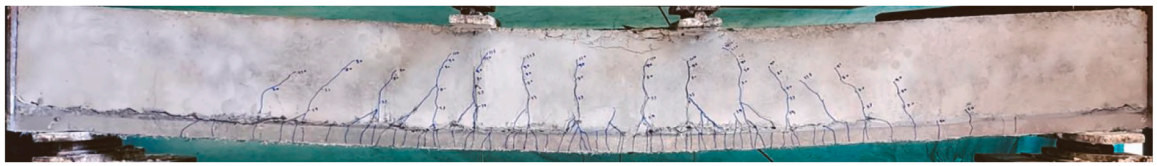


(c) Beam B-30%-S-30

Fig. 9. Cracking patterns at failure of beams of Group 2.



(e) Beam B-20%-S-40



(f) Beam B-20%-S-50

Fig. 10. Cracking patterns at failure of beams of Group 3.

compression zone reduces the ductility of the member. The ductility index of the control beam ($\mu_d = 4.63$) was the highest among all tested beams due to the high plastic deformation induced by the plastic behavior of the reinforcing steel after yield point.

For beams of Group 1, comparing to the reference beam, adding GFRP bars at tension side for B-0 %-N-0 led to a flexural failure at higher ultimate load, however, the ductility index reduced by 17.5 %. For beams B-20 %-N-0 and B-20 %-NS-0, prestressing of the GFRP bars led to lower ultimate deflection and reduced the ductility indices by 22 % and 18.8 %, respectively, comparing to BC. Although the strengthened beams with non-replaced cover of Group 1 were affected by the spalling and deterioration of the concrete cover, B-0 %-N-0 had higher ductility index comparing to B-20 %-N-0 and B-20 %-NS-0. This is attributed to the effect of prestressing which reduced the ductility of the prestressed beams. Despite the effect of prestressing of the GFRP bars of B-20 %-S-30, it had the highest ductility index of the strengthened beams of Group 1 ($\mu_d = 4.11$). The reason is that the SHCC replaced cover prevented B-20 %-S-30 to fail prematurely at low ultimate load/deflection due to debonding, it acted as a bonded prestressed beam until failure.

For Group 2, the ductility indices of B-0 %-S-30, B-10 %-S-30, B-20 %-S-30 and B-30 %-S-30 achieved 95 %, 93 %, 88 % and 84 %, respectively, of that achieved by the control beam. The ductility of these strengthened beams reduced by increasing the prestressing level. Beam B-0 %-S-0 recorded the highest ductility index among all strengthened beams as the SHCC replaced cover protected the beam from the effect of debonding and the zero prestreesing level allowed the beam to attain higher deflection than other beams. For Group 3, the ductility indices of B-20 %-S-30, B-20 %-S-40 and B-20 %-S-50 achieved 88 %, 90 % and 91 %, respectively, of that achieved by the control beam, respectively. It is obvious that the ductility of these beams increased slightly by increasing the thickness of the SHCC replaced cover.

3.4. Load crack-width behavior

For all tested beams, the maximum crack width within the constant moment zone was recorded during the test until failure. The maximum crack-width was measured at the level of the main steel of all beams. Fig. 14 shows the relationship between the applied load and the maximum crack-width of all tested beams. The control unstrengthened beam BC showed the maximum crack-width at ultimate load compared

Table 4
Test results summarize.

Group	Specimen	P_{cr}, kN	Yield point		Ultimate point		Ductility index
			P_y, kN	Δ_y, mm	P_u, kN	Δ_u, mm	
control	BC	18	62	10.3	78	47.7	4.63
Group 1	B−0 %-N−0	18	73	11.1	98	42.4	3.82
	B−20 %-N−0	26	79	8.1	108	29.2	3.61
	B−20 %-NS−30	37	83	7.3	117	27.5	3.76
	B−20 %-S−30	32	87	8.1	136	33.3	4.11
Group 2	B−0 %-S−30	24	77	10.3	124	45.7	4.43
	B−10 %-S−30	28	82	9.0	132	39.1	4.34
	B−30 %-S−30	40	93	7.9	147	31.1	3.93
Group 3	B−20 %-S−40	36	90	7.5	142	31.4	4.18
	B−20 %-S−50	39	92	7.7	148	32.5	4.22

P_{cr} = the recorded load at first crack; P_y = the load at yielding of main steel; Δy = the mid-span deflection at yielding of main steel; P_u = the ultimate load at failure; Δ_u = the mid-span deflection at ultimate load.

to the strengthened beams as it had the lowest reinforcement ratio and the lowest flexural stiffness. For strengthened beams with non-replaced cover B-0 %-N-0, B-20 %-N-0 and B-20 %-NS-30, a rapid increase in crack-width was observed after yield load of these beams. After yielding of steel bars, a higher strain rate was attained by the GFRP strengthening bars. The high strain rate and the low elastic modulus of the GFRP bars resulted in extensive elongation of the GFRP bars that couldn't be resisted by the surrounding non-replaced weak concrete cover which resulted in instant widening of crack widths. It was also noted that prior to yield of main steel, B-20 %-NS-30 without replaced cover recorded convergent crack widths at the same loading levels compared to B-20 %-S-30 with SHCC replaced cover. The effect of the deterioration of concrete cover after yielding of steel was obvious as B-20 %-NS-30 recorded higher increasing rate of crack widening, which indicates that the externally added SHCC layer without cover replacement failed to mitigate the effect of cover deterioration. For beams of Group 2, at the same load level, by increasing the prestressing level, maximum crack-width decreased. This is caused by the effect of prestressing that reduces the tensile strain recorded at the level of main steel. Beam B-30 %-S-30 with the highest prestressing level showed the lowest crack-width at ultimate load compared to all tested beams. Beams of Group 3 showed low rate of crack widening compared to the other strengthened beams as the increase of the SHCC layer thickness led to increase the flexural tensile strength of the beams in addition to the advantage of cover protection against spalling and deterioration.

3.5. Load-strain behavior (steel bars)

The load–strain curves of the main steel of all beams are shown in Fig. 15. Generally, the tensile strain propagation is governed by three consequent stages. For prestressed strengthened beams, the first stage started with an initial strain induced by the prestressing effect, while, ended with the first tensile crack at which the beam's stiffness starts to deteriorate. For the other beams without prestressing, the first stage showed the same manner except that there were no initial strains. The second stage started with lower stiffness until reaching the yield point which resulted in a higher strain rate for the consequent stage, whereas the third one ends with the maximum recorded load-carrying capacity at failure. All strengthened beams failed due to crushing of concrete at compression side preceded by yielding of the main steel but without rupture of the GFRP bars. Beams of Group 1 with non-replaced cover B-20 %-N-0 and B-20 %-NS-30 showed lower stiffness after yielding of main steel bars compared to B-20 %-S-30. This is caused by the effect of concrete cover spalling that turned the strengthened beams without cover replacement to behave as unbonded prestressed beams with lower strain rates [69,70]. For beams of Group 2, the higher the prestressing level was the lower the strain rate attained. Beams of Group 3, B-20 %-S-40 and B-20 %-S-50 showed a slight increase in the slope of the load-strain curve compared to B-20 %-S-30; this is attributed to the higher flexural stiffness induced by the additional gained resistance at flexural tensile zone.

3.6. Load-strain behavior (GFRP bars)

The load–strain curves of the GFRP bars of all beams are shown in Fig. 16. All prestressed strengthened beams started the test with the initial strain induced by the prestressing force applied to the GFRP bars prior to loading. Commonly, for all beams, the tensile strain growth is

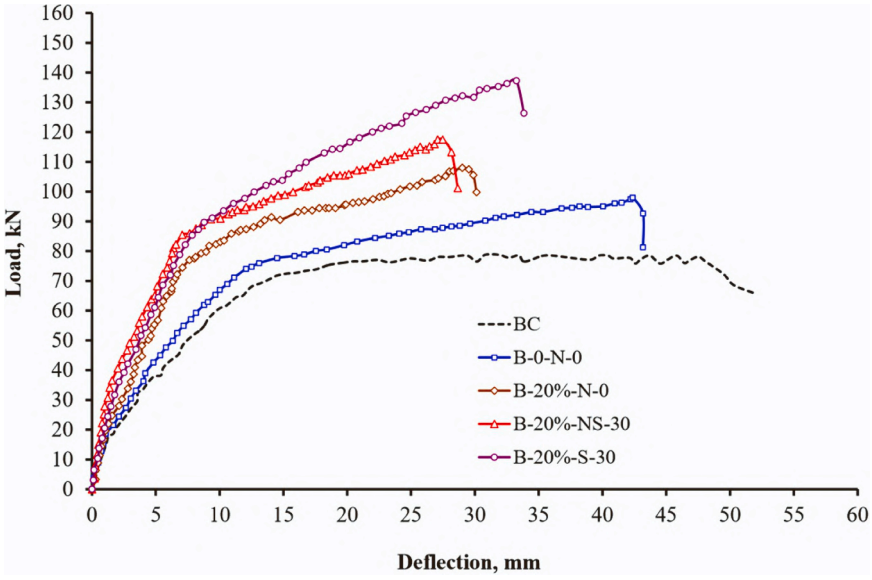


Fig. 11. Load-deflection curves for beams of Group 1.

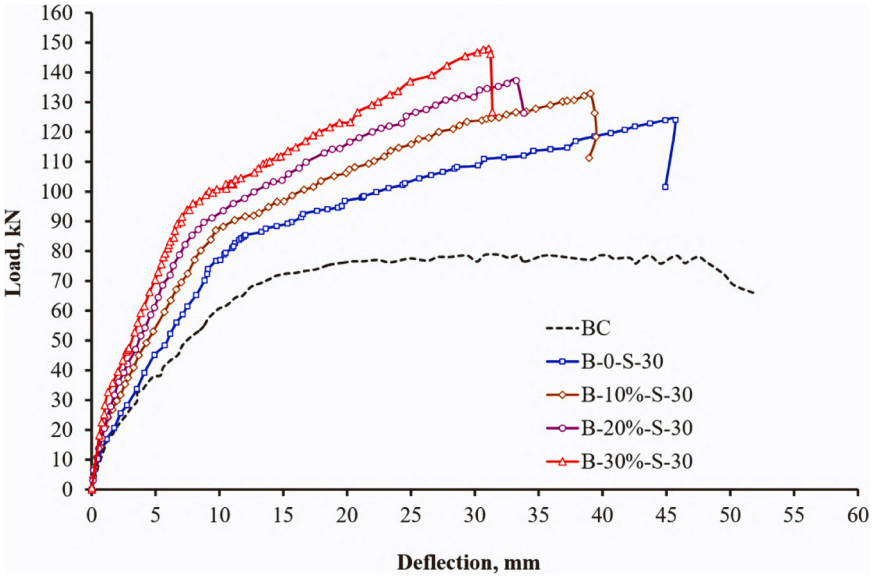


Fig. 12. Load-deflection curves for beams of Group 2.

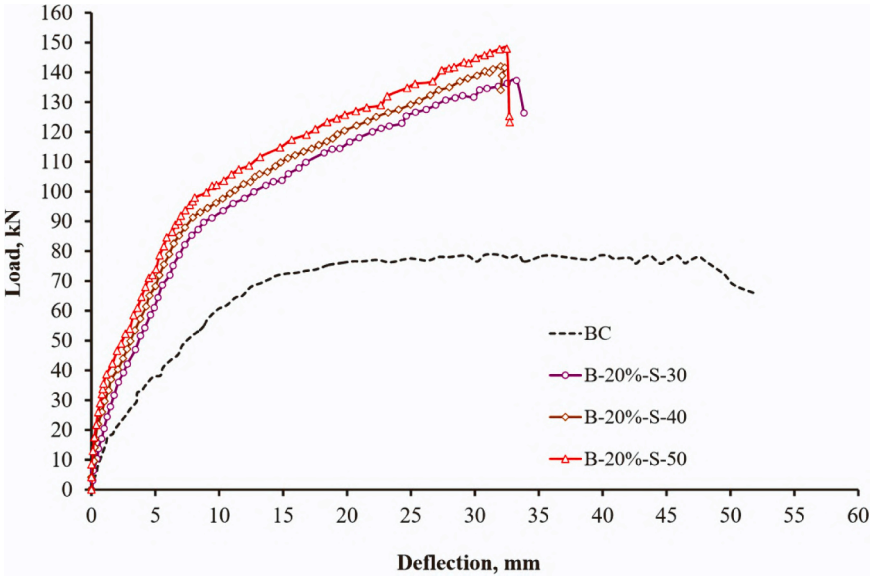


Fig. 13. Load-deflection curves for beams of Group 3.

characterized by three stages. The first stage (cracking stage) ended with the first tensile crack. The second stage (with lower stiffness) ended with the yield point, while the third one ends with the ultimate failure load. For Group 1, it was clear that the cover replacement by SHCC layer has an obvious effect on the load–strain behavior. For strengthened non-prestressed beams, comparing B-0 %-N-0 and B-0 %-S-30, the two beams showed almost the same stiffness (slope) until yield point of the main steel. After yield point, B-0 %-N-0 showed lower stiffness and lower maximum strain compared to B-0 %-S-30. For strengthened pre-stressed beams, B-20 %-N-0 and B-20 %-NS-30 showed a reduced post yield stiffness and lower ultimate strain compared to B-20 %-S-30. It is obvious that regardless of the prestressing level, the effect of spalling and deterioration of the concrete cover made the beams with non-replaced cover acting as unbonded prestressed system with lower stiffness until failure [69,70]. For beams of Group 2, by increasing the prestressing level, the strain rate of the beams decreased, and the ultimate maximum strain increased. This was caused by the attained mode of failure, all beams of Group 2 failed due to crushing of concrete at compression zone, therefore the increase in the prestress level resulted in a higher maximum GFRP stress at failure. The increase in the thickness of the SHCC layer for beams of Group 3 increased the beam's depth as well as the gained resistance at flexural tensile zone which led to lower strain values of the GFRP bars at the same load levels. As per load–strain relationships shown in Fig. 16, all strengthened beams failed prior to the ultimate strain of the GFRP bars (about 30,000 micro strain) due to crushing of concrete at compression zone.

3.7. Longitudinal strain distribution along beam's depth

During the test, five pi-gauges along the depth of the beam at the mid-span were employed to record the longitudinal strain values along beam's depth. As shown in Fig. 17, the strain distribution along the beam's depth at mid-span was monitored at the levels of cracking, service and at ultimate load; the service load was considered at 67 % of the ultimate load. As shown in Figs. 17-a to 17-c, the strain distributions were mostly linear for the first two levels, however, this was not the

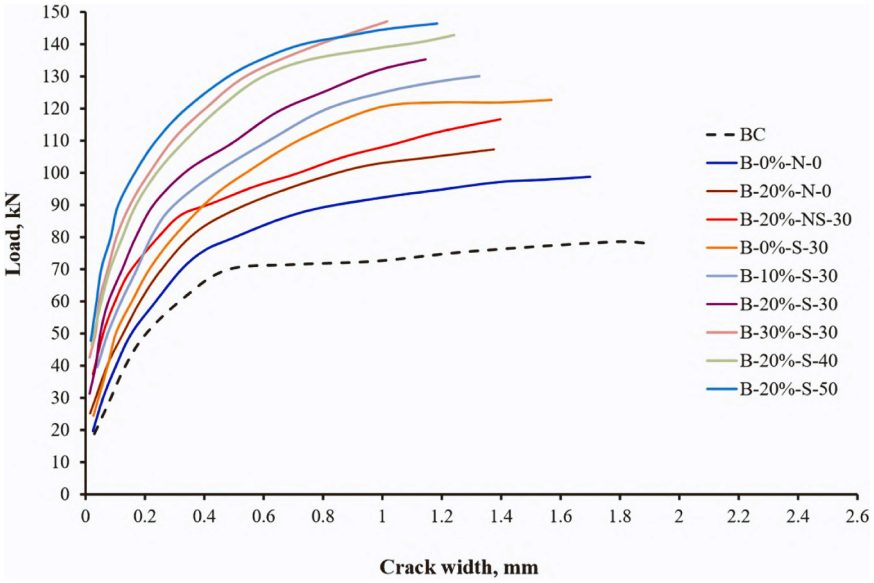


Fig. 14. Load vs maximum crack-width of all tested beams.

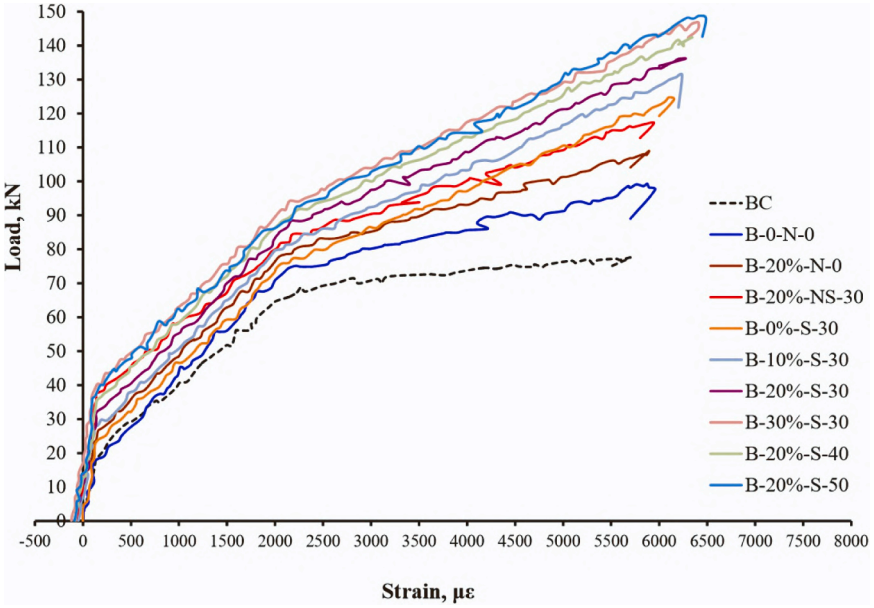


Fig. 15. Load-strain relationships of main steel for all tested beams.

same at the ultimate load level at which a sudden increase in the strain at the maximum tension fiber. This manner was observed post to yield of the main steel due to the relative strain initiated at the level of GFRP bars resulting in a non-linear strain distribution which nonconforms to the assumptions of plane compatibility. Although the anchoring plates could suppress the GFRP debonding from ends, debonding induced cracks and spalling of concrete cover were always observed after yield of tension steel due to the extensive elongation of the GFRP bars. At the time the spalling cracks were developing, the normal stresses became greater than the interfacial bond strength, therefore, the GFRP bars turned to be unbonded. As presented in Figs. 17-d to 17-i, beams of Groups 2 and 3 with SHCC replaced cover showed a similar behavior. This behavior can be described as follows; all monitored levels showed a linear strain distribution along beam's depth without any sudden variations of strain values which coincides with Euler-Bernoulli beam theory and indicates the perfect composite action gained by the cover replacement. The high strain capacity of the SHCC replaced cover (more than 0.03) can resist the high strain values attained by the GFRP bars post to yield preventing debonding induced by spalling of cover.

4. Capacity of PGFRP-strengthened beams

Based on the experimental results, two modes of failure were recorded for all beam specimens. The first is a flexural failure due to yielding of tensile steel followed by crushing of concrete at compression zone without spalling of the concrete cover without rupture of GFRP bars, while the second is a flexural failure post to steel yielding without rupture of GFRP bars but was accompanied with cover deterioration and spalling. The second mode of failure was prematurely triggered by the partial debonding of the GFRP bars (The bars were anchored at the beam's ends) that turned the beam to act as the unbonded prestressed systems with lower capacity. Due to the lack of bond, the stresses in the unbonded bars are averaged along the whole structure, which cannot be estimated using strain compatibility approach in the critical cross

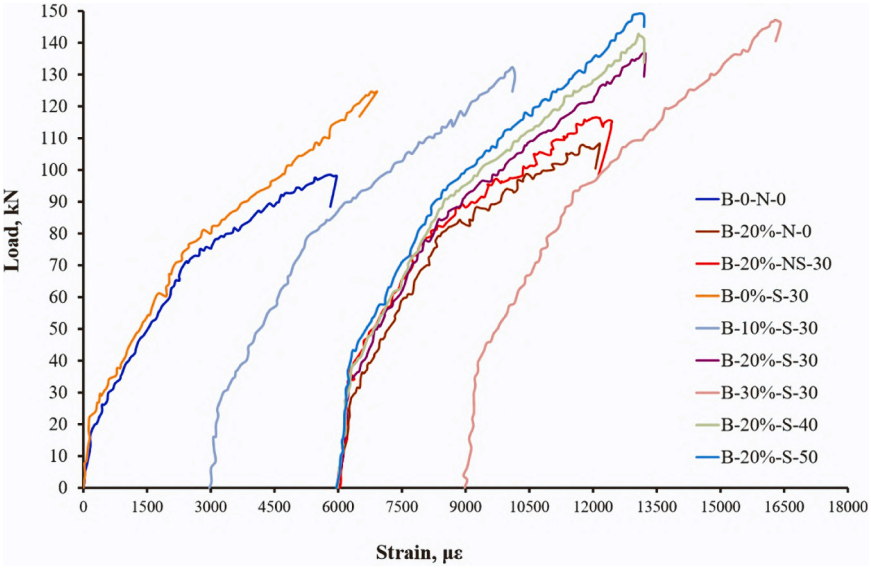


Fig. 16. Load-strain relationships of GFRP bars for all tested beams.

sections [87–89]. In this research, the analytical study was carried out only for beam specimens with SHCC replaced cover at which spalling of concrete cover did not take place until failure and the strain compatibility approach can be applied. For design purposes, the flexural capacity of the PGFRP-strengthened beams can be estimated based on analytical formulations.

The strain levels of reinforcement (Steel, GFRP bars) of prestressed beams pass through two stages to achieve the ultimate capacity of the beam. The first stage is applying the pretension force to the GFRP bars, while the second stage is applying the external load until failure. As previously mentioned in the experimental program, the pretension force was applied at 0 %, 10 %, 20 % and 30 % of the ultimate strain level of the GFRP bars. The pretension force can be expressed as follows:

$$P_e = \varepsilon_{pi} \times E_G \times A_b \tag{2}$$

Where; P_e is the effective prestressing applied force, $\varepsilon_{pi}$is the initial strain value (including sort term losses) pertaining to the applied prestressing force, E_G and A_b are the Young's modulus and the cross-sectional area of the GFRP bars, respectively. After application of the prestressing force, the eccentricity of this force from the center of the beam's section caused a negative bending moment. This negative moment is affecting the beam's cross section with removed concrete cover and leads to initial strains in concrete and steel reinforcement. The prestressing induced moment is assumed to be within the elastic cracked/non-cracked stage of the beam.

For the non-cracked section, the prestressing induced moment as well as strain levels of concrete and steel bars can be conducted by deducing the location of the section's neutral axis. As shown in Fig. 18-a, the neutral axis of the non-cracked section (C.G.1) can be located as follows:

$$y = \frac{nA'_s \times (d - d' + 0.5\ t_m) + b \times d \times 0.5\ (d + t_m) + nA_s \times 0.5\ (\varphi_s + t_m)}{nA'_s + b\ d\ + nA_s} \tag{3}$$

Where; y is the lever arm between the prestressing force and the center of the non-cracked section (C.G.1), n is the modular ratio which can be defined as the ratio between the Young's modulus of steel to the Young's modulus of concrete ($n = 10$ for non-cracked section), b is the width of the beam, d is the beam's total depth excluding the replaced concrete cover, d' is the concrete cover of the secondary steel, A_s is the main steel, A'_s is the secondary steel, t_m is the thickness of the SHCC layer, φ_s is the diameter of the main steel. For the non-cracked section, the stress level of concrete at the tension side is less than the tensile strength of concrete. The stress level of concrete at tension side and the tensile strength of concrete can be estimated as follows:

$$f_{tc} = p_e \left[\frac{y\ d + 0.5\, y\ t_m - y^2}{I_g} - \frac{1}{bd} \right] \leq f_{tcr} \tag{4-a}$$

$$I_g = I_c + I_s + I_{s'} \tag{4-b}$$

$$I_c = \frac{bd^3}{12} + bd \times (0.5d - y + 0.5t_m)^2 \tag{4-c}$$

$$I_s = nA_s \times (y_1 - 0.5t_m - 0.5\varphi_s)^2 \tag{4-d}$$

$$I_{s'} = nA'_s \times \ (d - d' + 0.5\ t_m - y)^2 \tag{4-e}$$

$$f_{tcr} = 0.62\sqrt{f_c'} \tag{5}$$

Where; f_{tc} is the maximum tensile stress acting on concrete, f_{tcr} is the tensile strength of concrete according to ACI 318–19 [74], p_e is the effective prestressing force, I_g is the second moment of area of the beam's section, I_c is the second moment of area of the concrete, I_s is the second moment of area of the main steel, I'_s is the second moment of area of the secondary steel, f_c' is the compressive strength of the standard concrete cylinder (150 ×300 mm). The prestressing induced moment ($M_{p.s.}$) in the case of non-cracked section can be obtained as follows:

$$M_{p.s.} = p_e \times y \tag{6}$$

For the cracked section, the concrete tensile stress exceeds its strength ($f_{tc} > f_{tcr}$), the prestressing induced moment as well as strain levels of concrete and steel bars can be estimated by locating the centroid of the section. To determine the centroid location, force stability equations based on the linear elastic distribution of the stresses along with beam's depth are solved to obtain the compression depth (c) as well as the maximum compressive stress acting on the concrete (f_{cc}). As shown in Fig. 18-b, the stability of forces can be expressed as follows:

$$P_e = F_{cc} + F_{cs} - F_{ts} \tag{7-a}$$

$$F_{cc} = \frac{1}{2} f_{cc} \times c \times b \tag{7-b}$$

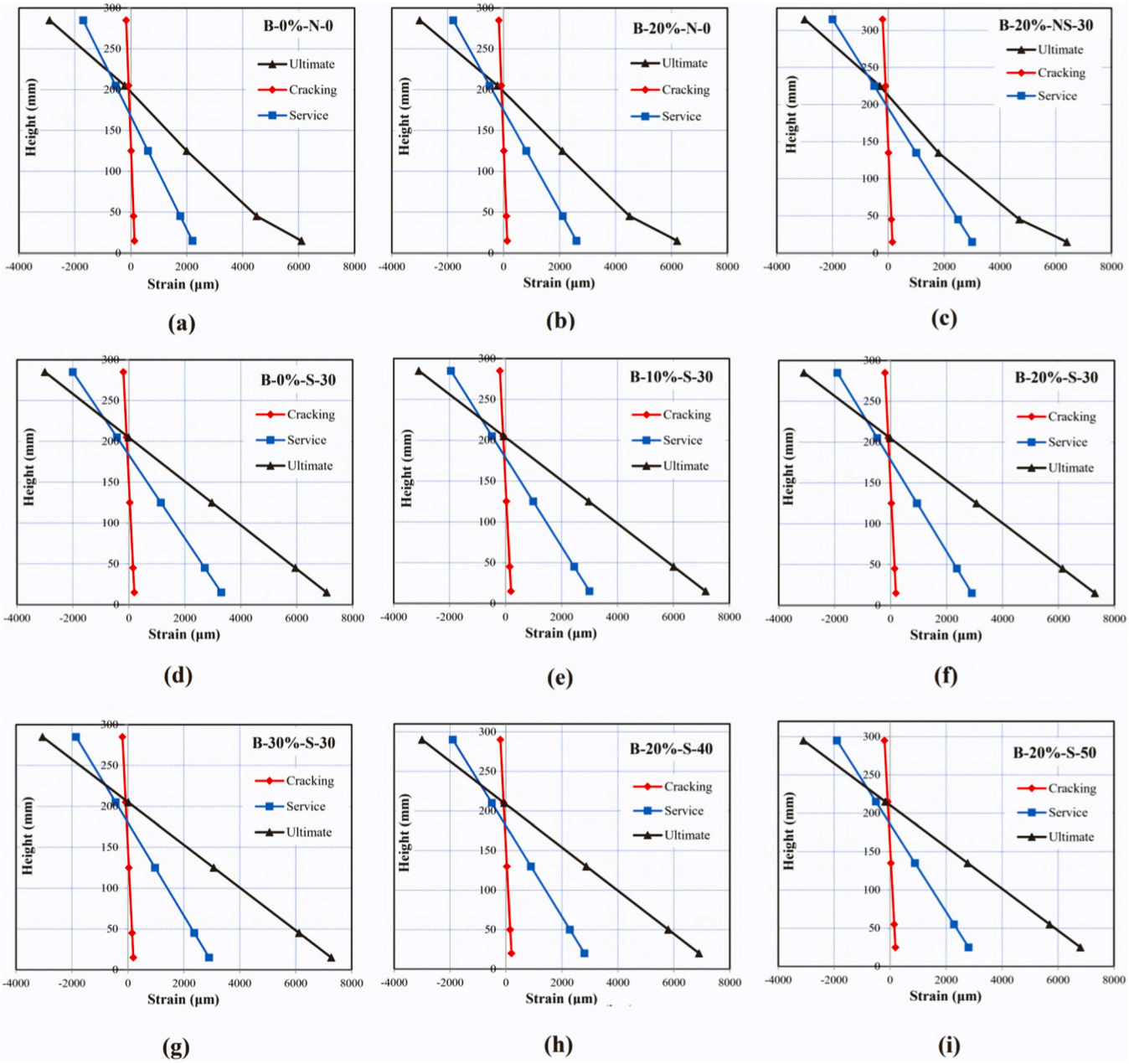


Fig. 17. Strain distribution along beam's depth at mid-span.

$$F_{cs} = n \times A_s' \times f_{cc} \times \left(\frac{c - 0.5\,\varphi_s}{c}\right) \tag{7-c}$$

$$F_{ts} = n \times A_s \times f_{cc} \times \left(\frac{d - c - d'}{c}\right) \tag{7-d}$$

Where; F_{cc} is the resultant force induced by the compressive stress of the concrete, F_{cs} is the resultant force induced by the compressive stress of the main steel, F_{ts} is the resultant force induced by the tensile stress of the secondary steel. As shown in Fig. 18-b and Fig. 18-c, the stability of the acting moments can be expressed as follows:

$$P_e \times (c + 0.5t_m) = F_{cc} \times 0.667\ c + F_{cs} \times (c - 0.5\,\varphi_s) + F_{ts} \times (d - c - d') \tag{8}$$

By solving Eqs. 7 and 8, the values of the compression depth (c) and the maximum compressive stress acting on the concrete (f_{cc}) can be obtained. The prestressed induced moment ($M_{p.s.}$) in the case of cracked section can be obtained as follows:

$$M_{p.s.} = P_e \times (c + 0.5t_m) \tag{9}$$

The second stage is applying the external loads until failure. Since the prestressing effect is a compression stress at the main steel zone, the main steel starts to be under tension in case the external applied moment exceeds the prestressed induced moment. Thus, the ultimate capacity of the beam can be estimated by adding the maximum resisting moment of the beam in the second stage to the prestressing induced moment of the first stage. As shown in Fig. 19, the maximum moment of the second stage can be estimated by applying the linear strain and force equilibrium assumptions. The equilibrium of the nominal internal forces can be estimated as per ACI 318–19 [74] as follows:

$$P_{eu} + F_{tsu} + F_{tm} = F_{ccu} + F_{csu} \tag{10-a}$$

$$F_{ccu} = 0.85 \times f_c' \times b \times \beta_1 c \tag{10-b}$$

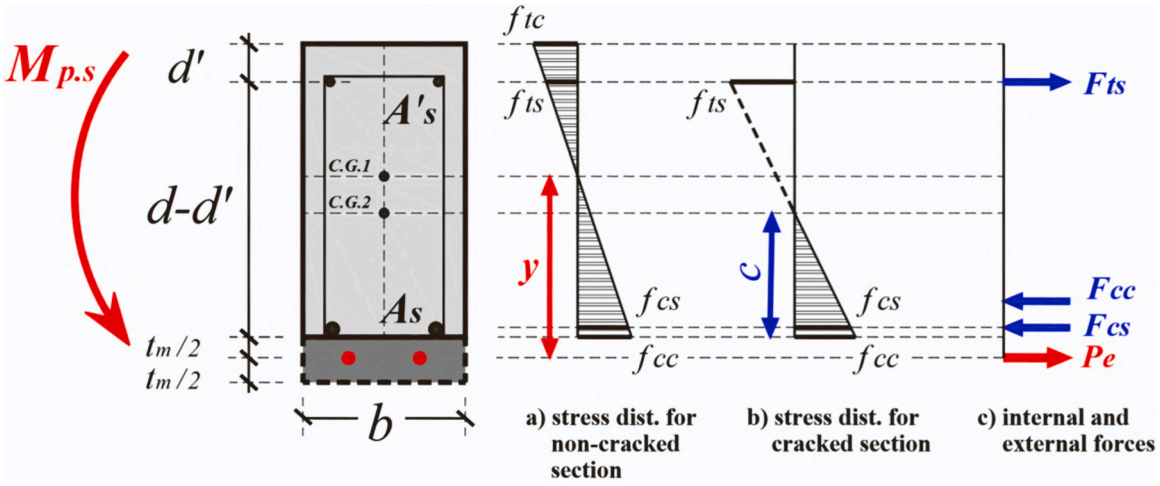


Fig. 18. Stress distribution along beam's depth of cracked/non-cracked section in the first stage.

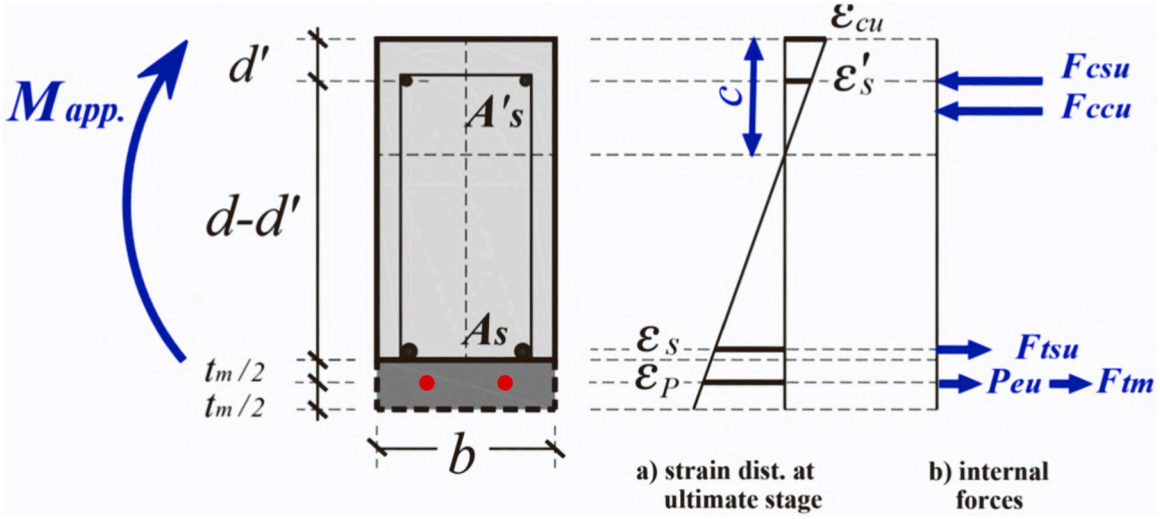


Fig. 19. Strain distribution along beam's depth in the second stage.

$$F_{csu} = A_s' \times \varepsilon_s' \times E_s \quad (10\text{-c})$$

$$F_{tsu} = A_s \times \varepsilon_s \times E_s \quad (10\text{-d})$$

$$P_{eu} = A_p \times \varepsilon_p \times E_G \quad (10\text{-e})$$

$$F_{tm} = (b \times t_m) \times f_m \quad (10\text{-f})$$

Where; F_{ccu} is the ultimate resultant force induced by the compressive stress of the concrete due to external loads, F_{csu} is the ultimate resultant force induced by the compressive stress of the secondary steel due to external loads, F_{ts} is the ultimate resultant force induced by the tensile stress of the main steel due to external loads, P_{eu} is the ultimate resultant force induced by the tensile stress of the GFRP bars due to external loads, F_{tm} is the ultimate resultant force induced by the tensile stress of the SHCC layer due to external loads,β_1 is coefficient for the equivalent rectangular concrete stress distribution as per ACI 318–19 [74] as listed in Table 5, $\varepsilon_s'$is the strain value of the secondary steel, $E_s$is Young's modulus of steel, $\varepsilon_s$is the strain value of the main steel, $\varepsilon_p$is the strain value of the GFRP bars which is induced by the external loading, f_m is the developed stress of the SHCC.

The ultimate strain values can be estimated based on the linear strain distribution along the beam's depth as follows:

Table 5
Values of the coefficient of the equivalent rectangular stress distribution (ACI 318–19).

f_c' (MPa)	β_1
$17 \le f_c' \le 28$	0.85
$28 < f_c' < 55$	$0.85 - \frac{0.05\ (f_c' - 28)}{7}$
$f_c' \ge 55$	0.65

$$\varepsilon_s = \frac{(d - c - 0.5\varphi_s)}{c} \times \varepsilon_{cu} \le \varepsilon_y \quad (11\text{-a})$$

$$\varepsilon_s' = \frac{(c - d')}{c} \times \varepsilon_{cu} \le \varepsilon_y \quad (11\text{-b})$$

$$\varepsilon_m = \frac{(d - c + 0.5t_m)}{c} \times \varepsilon_{cu} \le \varepsilon_{mu} \quad (11\text{-c})$$

$$\varepsilon_p = \frac{(d - c + 0.5t_m)}{c} \times \varepsilon_{cu} \le \left(\varepsilon_{pu} - \varepsilon_{pi}\right) \quad (11\text{-d})$$

Where; $\varepsilon_{cu}$is the ultimate compressive strain value of the concrete ($\varepsilon_{cu} = 0.003$), $\varepsilon_y$is the yield strain value of the steel, $\varepsilon_{mu}$is the ultimate strain value of the SHCC, $\varepsilon_{pu}$is the ultimate strain value of the GFRP bars. The

Young's modulus of the SHCC can be estimated based on the experimental results of the material tests in the current study by idealizing the tensile stress-strain relationship of the used SHCC as shown in Fig. 20. The developed stress level of the SHCC can be estimated as per the idealized stress-strain relationship as follows:

$$f_m = 8330 \times \varepsilon_m \quad \Rightarrow \quad f_m \leq 5.00\ MPa \tag{12-a}$$

$$f_m = 5.00 + (\varepsilon_m - 0.0006) \times 67 \quad \Rightarrow \quad 5.00 \leq f_m \leq 6.90\ MPa \tag{12-b}$$

The compression depth of the concrete (c) can be obtained by solving the previous force equilibrium equations. As shown in Fig. 19, the maximum flexural strength of the beam in the second stage (M_{II}) can be calculated as the summation of the moments of the internal forces as follows:

$$M_{II} = F_{ccu} \times (d - 0.5\beta_1 c + 0.5t_m) + F_{csu} \times (d - d\ ' + 0.5t_m) - 0.5\, F_{tsu} \times (\varphi_s + t_m) \tag{13}$$

Finally, the total ultimate moment capacity of the beam (M_U) can be calculated by adding the prestressing induced moment to the maximum resisting moment of the second stage.

$$M_U = M_{p.s.} + M_{II} \tag{14}$$

The presented analytical equations were applied to estimate the flexural capacity of six beam specimens at which the concrete cover was replaced with the SHCC layer, all are included in the experimental study of the current research. The predicted and the experimental ultimate loads are listed in Table 6. The comparison between the experimental and the predicted ultimate loads were within an acceptable tolerance. As listed in Table 6, the maximum experimental to predicted ultimate loads (P_U /P_p) value was 1.14, while the minimum value was 1.10.

5. Conclusions

This study aims to evaluate the effectiveness of a newly developed strengthening technique for beams at which GFRP bars were used at tension side. The studied parameters included the effect of different strengthening techniques, the thickness of the SHCC replaced cover as well as the applied prestressing level. In addition, a calculation model for design purposes was proposed to estimate the flexural capacity of the strengthened beams having SHCC replaced cover. Based on the experimental results, the following concluding remarks can be drawn:

1. Compared to the conventional NSM strengthened beams, the replacement of concrete cover by SHCC layer led to avoid premature bond induced failure. The SHCC layer showed a perfect interfacial bond with the substrate concrete, enhanced the composite action, eliminated the relative slippage, and acted as a perfect transition layer.
2. The SHCC replaced cover enhanced both the ultimate load and ductility of the strengthened beams compared to the conventional NSM. For 20 % prestressed strengthened beams of Group 1, the beam with cover replacement showed an increase in the ultimate load and the ductility index by 25.9 % and 13.8 %, respectively, compared to the beam without cover replacement (B-20 %-N-0).
3. The prestressing of GFRP bars enhanced the load carrying capacity, however, the ductility was negatively affected. By increasing the prestressing level from 0 to 30 %, the gain in load carrying capacity reached 18.5 %, however the loss in ductility attained 11.3 %.
4. By increasing the thickness of the SHCC, both the ultimate load and ductility were slightly enhanced. Beams with SHCC layer thicknesses of 40 and 50 mm showed an increase in the load carrying capacity of 4.4 % and 8.8 %, respectively, while the ductility indices increased by 1.7 % and 2.6 %, respectively, compared to the beam with 30 mm thickness. The increase in SHCC layer thickness over 30 mm did not show a significant enhancement in load capacity or ductility.
5. A prediction model to calculate the ultimate capacity of the strengthened beams with SHCC replaced cover was conducted. The predicted ultimate loads have a good consistency with the test results.

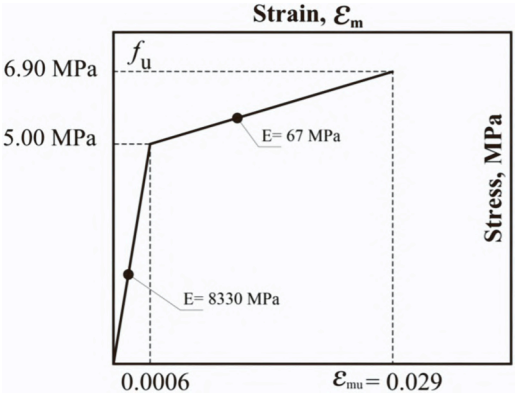


Fig. 20. Idealized stress-strain relationship of the SHCC in the current study.

Table 6
Comparison between the predicted and the experimental ultimate loads.

Beam	M_{UP} (kN.m)	P_p (kN)	P_U (kN)	P_U / P_p
B−0 %-S−30	58.1	111	124	1.11
B−10 %-S−30	61.3	117	132	1.13
B−20 %-S−30	64.6	123	136	1.10
B−30 %-S−30	67.9	129	147	1.14
B−20 %-S−40	66.5	127	142	1.12
B−20 %-S−50	69.1	132	148	1.12

M_{UP} = the predicted ultimate flexural moment capacity of the beam; P_p = the predicted ultimate load; P_U = the ultimate test load of the beam specimen.

The presented study is a first step to evaluate the efficiency of a new technique for FRP flexural strengthening and its ability to avoid premature debonding induced failures. For application of the newly developed technique in the field of construction, the presented study is limited to the studied dimensions, the number of tested beams, the strength of the materials, and the evaluated parameters. Future study having different anchoring system should be carried out to overcome several challenges in the application of this technique for beams with existing columns. In addition, further analysis (e.g. finite element modeling) should be performed to develop and promote this strengthening technique.

Authorship statement

All persons who meet authorship criteria are listed as authors, and all authors certify that they have participated sufficiently in the work to take public responsibility for the content, including participation in the concept, design, analysis, writing, or revision of the manuscript. Furthermore, each author certifies that this material or similar material has not been and will not be submitted to or published in any other publication before its appearance in the ***Engineering Structures***.

CRediT authorship contribution statement

Tarek F. El-Shafiey: Writing – review & editing, Supervision. **Mohamed Ezzat Ellithy:** Writing – original draft, Validation, Project administration, Methodology, Investigation, Data curation. **Ali Hassan:** Writing – review & editing, Supervision, Data curation, Conceptualization.

Declaration of Competing Interest

The authors declare that they have no known competing financial interests or personal relationships that could have appeared to influence the work reported in this paper.

Data availability

Data will be made available on request.

References

[1] Chajes JM, Finch WW, Thomson TA. Bond and force transfer of composite-material plates bonded to concrete. Struct J 1996;93(2):209–17.
[2] Barnes RA, Mays GC. Fatigue performance of concrete beams strengthened with CFRP plates. J Compos Constr 1999;3(2):63–72.
[3] Bakis Charles E, Lawrence CBank, Brown Vlet, Cosenza Edoardo, Davalos JF, Lesko JJ, et al. Fiber-reinforced polymer composites for construction – State-of-the-art review. J Compos Constr 2002;6(2):73–87.
[4] Gosbell T. Strengthening of the West Gate Bridge approach span, Melbourne. Struct Eng Int 2002;12(1):14–6.
[5] G. Al-Bayati, R. Al-Mahaidi, Torsional strengthening of concrete members using CFRP composites: a state-of-the-art review. In: Proceedings of the fourth Asia-Pacific conference on FRP in structures (APFIS 2013) 11–13 December 2013, Melbourne, Australia; 2013.
[6] Belarbi A, Acun B. FRP systems in shear strengthening of reinforced concrete structures. Procedia Eng 2013;57:2–8.
[7] Zaman A, Gutub SA, Wafa MA. A review on FRP composites applications and durability concerns in the construction sector. J Reinf Plast Compos 2013;32(24):1966–88.
[8] Bournas DA, Pavese A, Tizani W. Tensile capacity of FRP anchors in connecting FRP and TRM sheets to concrete. Eng Struct 2015;82:72–81.
[9] Ou Y, Zhu D. Tensile behavior of glass fiber reinforced composite at different strain rates and temperatures. Constr Build Mater 2015;96:648–56.
[10] A. Remennikov, M. Goldston, M.N. Sheikh, Impact performance of concrete beams externally bonded with carbon FRP sheets, Mechanics of Structures and Materials: Advancements and Challenges–Hao & Zhang (Eds). In: conference: proceedings of the twenty fourth Australian conference on the mechanics of structures and materials (ACMSM24), At Perth, Australia; 2016.
[11] Osman Bashir H, Wu Erjun, Ji Bohai, Abdulhameed Suhaib S. Repair of pre-cracked reinforced concrete (RC) Beams with openings strengthened using FRP sheets under sustained load. Int J Concr Struct Mater 2017;11(1):171–83.
[12] Sorrentino L, Turchetta S, Bellini C. In process monitoring of cutting temperature during the drilling of FRP laminate. Compos Struct 2017;168:549–61.
[13] Huo Jingsi, Li Zhi, Zhao Lingyu, Liu Jintong, Xiao Yan. Dynamic behavior of carbon fiber-reinforced polymer-strengthened reinforced concrete beams without stirrups under impact loading. Acids Struct J 2018;115(3):775–87.
[14] Bhong M, Khan TK, Devade K, Krishna BV, Sura S, Eftikhaar HK, et al. Review of composite materials and applications. Mater Today: Proc 2023.
[15] Crasto AS, Kim RY, Fowler C, Mistretta JP. Rehabilitation of concrete bridge beams with externally-bonded composite plates. Part I. First Int Conf Compos Infrastruct Natl Sci Found Natl Sci Found 1996.
[16] A. Hutchinson, H. Rahimi, Flexural strengthening of concrete beams with externally bonded FRP reinforcement. In: proceedings of the second international conference on advanced composite materials in bridges and structures, ACMBS-II, Montreal; 1996.
[17] Heffernan P, Erki M. Equivalent capacity and efficiency of reinforced concrete beams strengthened with carbon fibre reinforced plastic sheets. Can J Civ Eng 1996;23(1):21–9.
[18] Teng JG, Chen JF, Smith ST, Lam L. Behaviour and strength of FRP-strengthened RC structures: a state-of-the-art review. Proc Inst Civ Eng-Struct Build 2003;156(1):51–62.
[19] Ceci AM, Casas JR, Ghosn M. Statistical analysis of existing models for flexural strengthening of concrete bridge beams using FRP sheets. Constr Build Mater 2012;27(1):490–520.
[20] Kara IF, Ashour AF. Flexural performance of FRP reinforced concrete beams. Compos Struct 2012;94(5):1616–25.
[21] Al-Kamaki YS, Al-Mahaidi R, Bennetts I. Strength model for heat-damaged reinforced concrete circular columns confined with carbon fibre reinforced polymer fabrics. J Reinf Plast Compos 2015;34(22):1833–55.
[22] Megahed FA, Seleem MH, Badawy AAM, Sharaky IA. The flexural response of RC beams strengthened by EB/NSM techniques using FRP and metal materials: a state-of-the-art review. Innov Infrastruct Solut 2023;8(11):289.
[23] Chaallal O, Nollet MJ, Perraton D. Experimental investigation of RC beams strengthened in flexure with externally-bonded CFRP strips 1997.
[24] Duarte P, Correia JR, Ferreira JG, Nunes F, Arruda MRT. Experimental and numerical study on the effect of repairing reinforced concrete cracked beams strengthened with carbon fibre reinforced polymer laminates. Can J Civ Eng 2014;41(3):222–31.
[25] Morsy AM, El-Tony EM, El-Naggar M. Flexural repair/strengthening of pre-damaged RC beams using embedded CFRP rods. Alex Eng J 2015;54(4):1175–9.
[26] Shukri AA, Hosen MA, Muhamad R, Jumaat MZ. Behaviour of precracked RC beams strengthened using the side-NSM technique. Constr Build Mater 2016;123:617–26.
[27] Banjara NK, Ramanjaneyulu K. Experimental and numerical investigations on the performance evaluation of shear deficient and GFRP strengthened reinforced concrete beams. Constr Build Mater 2017;137:520–34.
[28] Bakar MBC, Muhammad Rashid RS, Amran M, Saleh Jaafar M, Vatin NI, Fediuk R. Flexural strength of concrete beam reinforced with CFRP Bars: a review. Materials 2022;15(3):1144.
[29] Li X, Gu X, Song X, Ouyang Y, Feng Z. Contribution of U-shaped strips to the flexural capacity of low-strength reinforced concrete beams strengthened with carbon fibre composite sheets. Compos Part B Eng 2013;45(1):117–26.
[30] Chen C, Wang X, Sui L, Xing F, Chen X, Zhou Y. Influence of FRP thickness and confining effect on flexural performance of HB-strengthened RC beams. Compos Part B Eng 2019;161:55–67.
[31] Yazdani N, Aljaafreh T, Beneberu E. Concrete beam flexural strengthening with anchored pre-saturated CFRP laminates. Compos Struct 2020;235:111733.
[32] Ali Alnadher, Abdalla Jamal, Hawileh Rami, Galal Khaled. CFRP mechanical anchorage for externally strengthened RC beams under flexure. Phys Procedia 2014;55:10–6.
[33] Hawileh Rami A, Assad Maha, Abdalla Jamal A. Effect of increasing the number of anchors on the flexural performance of FRP-strengthened RC beams. Procedia Struct Integr 2024;54:287–93.
[34] De Lorenzis L, Teng JG. Near-surface mounted FRP reinforcement: an emerging technique for strengthening structures. Compos B Eng 2007;38:119–43.
[35] Stone D, Tumialan G, Nanni A, Parretti R. Near-surface mounted FRP reinforcement: application of an emerging technology. Concrete 2002;36.
[36] Hawileh R. Nonlinear finite element modeling of RC beams strengthened with NSM FRP rods. Constr Build Mater 2011;27:461–71.
[37] Zaman A, Gutub SA, Wafa MA. A review on FRP composites applications and durability concerns in the construction sector. J Reinf Plast Compos 2013;32.
[38] Zhang Shi Shun, Tao Yu, Chen GM. Reinforced concrete beams strengthened in flexure with near-surface mounted (NSM) CFRP strips: Current status and research needs. Compos Part B: Eng 2017;131:30–42.
[39] R. Kotynia, Analysis of the flexural response of NSM FRP-strengthened concrete beams. In: Proceedings, eighth international conference on fibre reinforced plastics for reinforced concrete structures (FRPRCS-8); 2007. Patras, Greece, July 16 to 18; 2007.
[40] D.G. Novidis, S.J. Pantazopoulo, Beam tests of NSM FRP laminates in concrete. In: Proceedings, eighth international conference on fibre reinforced plastics for reinforced concrete structures; 2007. Patras, Greece, July 16–18; 2007.
[41] Teng JG, De Lorenzis L, Wang B, Rong L, Wong TN, Lam L. Debonding failures of RC beams strengthened with near-surface mounted CFRP strips. J Compos Constr 2006;10(2):92–105.
[42] Barros JAO, Costa IG, Ventura-Gouveia A. CFRP flexural and shear strengthening technique for RC beams: experimental and numerical research. Adv Struct Eng 2011;14(3):551–71.
[43] Peng H, Zhang JR, Cai CS, Liu Y. An experimental study on reinforced concrete beams strengthened with prestressed near surface mounted CFRP strips. Eng Struct 2014;79:222–33.
[44] Jung WT, Park JS, Kang JY, Keum MS. Flexural behavior of concrete beam strengthened by near-surface mounted CFRP reinforcement using equivalent section model. Adv Mater Sci Eng 2017;16.
[45] Seracino Rudolf, Jones Nicola M, Ali MS, Page Mark W, Oehlers Deric J. Bond strength of near-surface mounted FRP strip-to-concrete joints. J Compos Constr 2007;11(4):401–9.
[46] Bilotta A, Ceroni F, Di Ludovico M, Nigro E, Pecce M, Manfredi G. Bond efficiency of EBR and NSM FRP systems for strengthening concrete members. J Compos Constr 2011;15(5):757–72.
[47] Cruz Sena, Manuel José, Oliveira Barros Joaquim António. Bond between nearsurface mounted carbon-fiber-reinforced polymer laminate strips and concrete. J Compos Constr 2004;8(6):519–27.
[48] De Lorenzis, Andrea Rizzo Laura, Antonio La Tegola. A modified pull-out test for bond of near-surface mounted FRP rods in concrete. Compos Part B: Eng 2002;33(8):589–603.
[49] Novidis D, Pantazopoulou SJ, Tentolouris E. Experimental study of bond of NSM-FRP reinforcement. Constr Build Mater 2007;21(8):1760–70.
[50] Soliman Shehab M, El-Salakawy Ehab, Benmokrane Brahim. Bond performance of near-surface-mounted FRP bars. J Compos Constr 2010;15(1):103–11.
[51] Al-Mahmoud Firas, Castel Arnaud, François Raoul, Tourneur Christian. Anchorage and tension-stiffening effect between near-surface-mounted CFRP rods and concrete. Cem Concr Compos 2011;33(2):346–52.
[52] ACI Committee 440.2R-08, Guide for the design and construction of externally bonded FRP systems for strengthening concrete structures. American Concrete Institute, Farmington Hills, Michigan, USA; 2008.
[53] Badawi Moataz, Soudki Khaled. Flexural strengthening of RC beams with prestressed NSM CFRP rods–experimental and analytical investigation. Constr Build Mater 2009;23:3292–300.
[54] Peng Hui, Zhang Jianren, Cai CS, Liu Yang. An experimental study on reinforced concrete beams strengthened with prestressed near surface mounted CFRP strips. Eng Struct 2014;79:222–33.
[55] Sokairge, Hesham, Elgabbas Fareed, Elshafie Hany. Structural behavior of RC beams strengthened with prestressed near surface mounted technique using basalt FRP bars. Eng Struct 2022;250:113489.

[56] Cristian Sabau, Popescu Cosmin, Sas Gabriel, Wittrup Schmidt Jacob, Blanksvärd Thomas, Täljsten Björn. Strengthening of RC beams using bottom and side NSM reinforcement. Compos Part B: Eng 2018;149:82–91.
[57] Haddad Rami H, Yaghmour Emad M. Side NSM CFRP strips with different profiles for strengthening reinforced concrete beams. J Build Eng 2020;32:101772.
[58] Zhang SS, Ke Y, Smith ST, Zhu HP, Wang ZL. Effect of FRP U-jackets on the behaviour of RC beams strengthened in flexure with NSM CFRP strips. Compos Struct 2021;256:113095.
[59] Khalil AEA, Atta AM, Hassan A, Abd-Elaaty AH. Flexural strength recovery of RC one-way slabs having cut-outs using NSM-SHCC plates. Eng Struct 2022;258:114149.
[60] Afefy Hamdy, Kassem Nesreen, Hussein Mohamed. Enhancement of flexural behaviour of CFRP-strengthened reinforced concrete beams using engineered cementitious composites transition layer. Struct Infrastruct Eng 2015;11(8):1042–53.
[61] Li M, Li VC. High-early-strength ECC for rapid durable repair: material properties. Acids Mater J 2011;108(1).
[62] Zhang Z, Qin F, Ma H, Xu L. Tailoring an impact resistant engineered cementitious composite (ECC) by incorporation of crumb rubber. Constr Build Mater 2020;262:120116.
[63] Li M, Li VC. Cracking and healing of engineered cementitious composites under chloride environment. Acids Mater J 2011;108(3):333.
[64] Zhang Z, Zhang Q. Matrix tailoring of engineered cementitious composites (ECC) with non-oil-coated, low tensile strength PVA fiber. Constr Build Mater 2018;161:420–31.
[65] Li VC, Wu C, Wang S, Ogawa A, Saito T. Interface tailoring for strain-hardening polyvinyl alcohol-engineered cementitious composite (PVA-ECC). Mater J 2002;99(5):463–72.
[66] Zhang ZG, Hu J, Ma H. Feasibility study of ECC with self-healing capacity applied on long-span steel bridge deck overlay. Int J Pavement Eng 2019;20(8):884–93.
[67] Zhou J, Pan J, Leung CKY. Mechanical behavior of fiber-reinforced engineered cementitious composites in uniaxial compression. J Mater Civ Eng 2015;27(1(():04014111.
[68] Zhang Z, Zhang Q, Li VC. Multiple-scale investigations on self-healing induced mechanical property recovery of ECC. Cem Concr Compos 2019;103:293–302.
[69] Lepech M, Li VC. Long term durability performance of engineered cementitious composites. Restor Build Monum 2006;12(2):119–32.
[70] Shan He, Shozab Mustafa, Chang Ze, Liang Minfei, Schlangen Erik, Luković Mladena. Ultra-thin strain hardening cementitious composite (SHCC) layer in reinforced concrete cover zone for crack width control. Eng Struct 2023;292:116584.
[71] Khan MIqbal, Abbass Wasim. Flexural behavior of high-strength concrete beams reinforced with a strain hardening cement-based composite layer. Constr Build Mater 2016;125:927–35.
[72] Khalil A, Etman E, Atta A, Essam M. Behavior of RC beams strengthened with strain hardening cementitious composites (SHCC) subjected to monotonic and repeated loads. Eng Struct 2017;140:151–63.
[73] Hassan A, Ellithy M, El-Shafiey TF. Upgrading the shear strength of reinforced concrete corbels using strain hardening cementitious composites. Eng Struct 2022;273:115047.
[74] ACI Committee 3182019. Building code requirements for structural concrete (ACI 318–19) and commentary (ACI 318R-19). American Concrete Institute, Farmington Hills, MI. p. 519.
[75] Li Xia, Zhou Chang, Cheng Yi, Wang Wenwei. Shear properties of a novel wave-shaped shear connector for thin HPFRCC-steel composite structures. Mech Adv Mater Struct 2023:1–15.
[76] Li VC. Tailoring ECC for special attributes: a review. Int J Concr Struct Mater 2012;6:135–44.
[77] ASTM, Designation: C39/C39M. Standard test method: compressive strength of Cylindrical Concrete Specimens; 2010.
[78] Japan Society of Civil Engineers JSCE. Recommendations for design and construction of high performance fiber reinforced cement composite with multiple fine cracks (HPFRCC). Concr Eng Ser 2008;82.
[79] Kunieda M, Hussein M, Ueda N, Nakamura H. Enhancement of crack distribution of UHP-SHCC under axial tension using steel reinforcement. J Adv Concr Technol 2010;8(1):49–57.
[80] ASTM, Designation: A370−19. standard test methods and definitions for mechanical testing of steel products; 2019.
[81] ASTM, Designation: D 7205–7206. Standard test method for tensile properties of fiber reinforced polymer matrix composite bars; 2006.
[82] Huang Hui, Bin Jia, Jie Lian, Wen-Wei Wang. Experimental investigation on the tensile performance of resin-filled steel pipe splices of BFRP bars. Constr Build Mater 2020;242:118018.
[83] Yang DS, Park SK, Neale KW. Flexural behaviour of reinforced concrete beams strengthened with prestressed carbon composites. Compos Struct 2009;88(4):497–508.
[84] Saafi M, Toutanji H. Flexural capacity of prestressed concrete beams reinforced with aramid fiber reinforced polymer (AFRP) rectangular tendons. Constr Build Mater 1998;12(5):245–9.
[85] Du XL, Wang ZH, Liu JB. Flexural capacity of concrete beams prestressed with carbon fiber reinforced polymer (CFRP) tendons. Adv Mater Res 2011;168:1353–62.
[86] Park R. Evaluation of ductility of structures and structural assemblages from laboratory testing. Bull NZ Soc Earthq Eng 1989;22(3):155–66.
[87] Roberts-Wollmanm CL, Kreger ME, Rogowsky DM, Breen JB. Stresses in external tendons at ultimate. Acids Struct J 2005;102(2):206.
[88] He ZQ, Liu Z. Stresses in external and internal unbonded tendons: unified methodology and design equations. J Struct Eng 2010;136(9):1055–65.
[89] Dall'Asta A, Ragni L, Zona A. Simplified method for failure analysis of concrete beams prestressed with external tendons. J Struct Eng 2007;133(1):121–31.